7-29-2003

Tidal Corrections for TOPEX Altimetry in the Coral Sea and Great Barrier Reef Lagoon: Comparisons With Long-Term Tide Gauge Records

D.M. Burrage
University of Southern Mississippi

C.R. Steinberg
James Cook University

L.B. Mason
James Cook University

L. Bode
James Cook University

Tidal corrections for TOPEX altimetry in the Coral Sea and Great Barrier Reef Lagoon: Comparisons with long-term tide gauge records

D. M. Burrage,[1,2,3] C. R. Steinberg,[1,2] L. B. Mason,[4,2] and L. Bode[5,2]

Received 17 May 2000; revised 5 August 2002; accepted 4 March 2003; published 29 July 2003.

[1] The well-known capability of TOPEX/Poseidon altimetry to map sea levels precisely in the deep oceans motivates its application to the topographically complex Coral Sea and NE Australian continental margin. We assess several global tidal models for correcting TOPEX altimetry in the Coral Sea and find CSR3.0 offers good overall performance, based on comparisons of model-predicted and tide gauge harmonic constituents. Using CSR3.0 tidal corrections, we evaluate residual Sea Surface Height (SSH) Root Mean Square (RMS) variability and residual M2 tidal alias errors. Away from large reefs and islands, CSR3.0 amplitude and phase errors for M2 are typically less than 5 cm and 8 deg, respectively, with RMS tidal errors of 5 cm or less and RMS SSH residuals approximating 10 cm. Since model deficiencies appear in the macro-tidal region of the Southern Great Barrier Reef Lagoon, near Broad Sound, we employ a high-resolution hydrodynamic model in this area to compute the tidal corrections. Predicted M2 amplitude and phase in this region are within 3 cm and 5 deg of observations, RMS errors are mostly under 4 cm and coastal RMS SSH residuals are as low as 15 cm, in spite of coastal trapped waves and submesocale eddies in the Lagoon. Daily and monthly smoothed SSH residual time series, respectively, yield optimal lagged correlations with in situ sea level data in the range 0.3–0.9 and 0.6–0.9 for locations spanning the Coral Sea and in the Lagoon. Lag correlations of monthly smoothed Geostrophic Current Anomalies derived from TOPEX SSH gradients with long-term currents from the continental slope yield optimal correlations of 0.5 and 0.8, respectively, near Jewell (lat 14 deg S) and Myrmidon Reef (19 deg S). Our results demonstrate that low-frequency sea level and geostrophic current variations can be reliably observed using altimetry over the Coral Sea and NE Australian continental slope, and for selected locations on the continental shelf, if appropriate tide correction models are employed. *INDEX TERMS:* 4243 Oceanography: General: Marginal and semienclosed seas; 4275 Oceanography: General: Remote sensing and electromagnetic processes (0689); 4556 Oceanography: Physical: Sea level variations; 4560 Oceanography: Physical: Surface waves and tides (1255); *KEYWORDS:* TOPEX, altimetry, tides, corrections, Coral Sea, Great Barrier Reef

Citation: Burrage, D. M., C. R. Steinberg, L. B. Mason, and L. Bode, Tidal corrections for TOPEX altimetry in the Coral Sea and Great Barrier Reef Lagoon: Comparisons with long-term tide gauge records, *J. Geophys. Res.*, *108*(C7), 3241, doi:10.1029/2000JC000441, 2003.

1. Introduction

[2] High quality sea level data have been available from the TOPEX/Poseidon altimeters since satellite launch in August 1992. By using hybrid models that fit altimetry data to empirical functions derived from numerical hydrodynamic models [*Cartwright and Ray*, 1990, 1991; *Desai and Wahr*, 1994; *Eanes and Bettadpur*, 1995; *Le Provost et al.*, 1998], deep ocean tides have been estimated with unprecedented precision and accuracy. This achievement stems directly from the TOPEX orbit design, which allows tidal aliases to be separated [*Parke et al.*, 1987], from precise satellite tracking and orbit determination, and from advances in modeling and data assimilation. Early successes in comparing tidally corrected altimetric Sea Surface Height fields (SSH here and subsequently refers exclusively to altimeter-derived data) with ''reference'' tide gauges [e.g., *Le Provost*, 1994] spurred rapid development of both tidal models and sea level observing systems. Deep ocean sea levels can now be estimated with a Root Mean Square (RMS) precision of about 2 cm, approaching and even exceeding that attainable using conventional tide gauges. We are now moving into a new operational era with the

[1]Australian Institute of Marine, Science, Townsville, Queensland, Australia.
[2]Cooperative Research Centre for the Great Barrier Reef World Heritage Area, CRC Reef Research Centre, Ltd., James Cook University, Townsville, Queensland, Australia.
[3]Now at Department of Marine Science, University of Southern Mississippi, Stennis Space Center, Mississippi, USA.
[4]School of Engineering, James Cook University, Townsville, Queensland, Australia.
[5]School of Mathematical and Physical Sciences, James Cook University, Townsville, Queensland, Australia.

0148-0227/03/2000JC000441

implementation of the TOPEX follow-on mission and the recent launch of JASON-1 and renewed efforts to meet the "1 cm" challenge [*Ménard*, 1999]. It is thus appropriate to consider utilizing the tidally corrected altimetry for studies in the marginal seas and near the coasts, where many new operational applications will be focused, and to reassess the performance of the existing tidal models in this context.

[3] Possible applications in these areas are just beginning to be explored [*Foreman et al.*, 1998; *Kantha et al.*, 1994]. An important exception is the Mediterranean Sea, studies of which are well advanced [*Bonnefond et al.*, 1995; *Larnicol et al.*, 1995, *Ayoub et al.*, 1998]. This possibility is particularly attractive for work in topographically complex marginal seas such as the Coral Sea. The associated tidal and low-frequency circulation are spatially complex, and a large number of conventional in situ moorings would be needed to span and resolve the Coral Sea circulation adequately. This complexity, enhanced by numerous coral reefs and islands, also presents significant challenges in mapping tidal constituents and mesoscale circulation using altimetry. These include adequately resolving tidal gradients, computing accurate tidal corrections and avoiding aliasing effects. New challenges arise near the coasts from dynamical processes such as coastal-trapped waves that may be aliased by the TOPEX and JASON return period (10 days). Variations in the width of the NE Australian continental shelf and the massive Great Barrier Reef (GBR) add further complexity. Fortunately, the region also presents opportunities to help meet these challenges. A high precision network of SEAFRAME (henceforth, SF) acoustic tide gauges was established by the National Tidal Facility (NTF) at island, reef and coastal locations in the Western Pacific and along Australian coastlines prior to TOPEX launch. Regional tidal models that have been specifically designed to address and resolve the topographic complexity of the GBR environment are also available.

[4] A skillful tidal model is obviously required to correct altimetry data for use in low-frequency circulation studies. However, verifying model performance does present some difficulties. In comparisons with in situ sea level data, local influences must be considered, especially if the site is distant from the altimeter ground track. For coastal applications we should avoid making comparisons close to model boundaries constrained by in situ measurements (the *Schwiderski* [1980] model was strongly constrained by such data along the shelfbreak), while obvious difficulties also arise due to the limited grid resolution (0.5 deg) of the standard global tidal models, CSR3.0 [*Eanes and Bettadpur*, 1995] and FES 95.2 [*Le Provost et al.*, 1998]. Computational techniques are available to improve grid resolution near the coast (as in FES 95.2), but these finer scale results are not generally available.

[5] In certain coastal areas, especially in the GBR, sufficient accuracy and resolution can only be obtained by using high-resolution regional hydrodynamic models [e.g., *Bode and Mason*, 1995; *Bode et al.*, 1997]. Such models may be forced at open boundaries by in situ data where available, and validated or tuned by using in situ data from stations interior to the model domain. Another approach being explored uses altimetry-derived deep ocean tide models to force one-way nested regional numerical hydrodynamic models to propagate the tide into the coast [*Burrage et al.*, 1998; *Kantha et al.*, 1994; L. H. Kantha, unpublished manuscript, Relocatable Modeling Environment CCAR/CAST/NAVOCEANO: Altimetry in Marginal, Semi-Enclosed and Coastal Seas, Mississippi State University, Center for Air Sea Technology]. This concept is particularly applicable to the GBR, where loss of lock as the altimeter traverses emergent coral structures can cause significant data "dropouts." This effect inherently limits coastal application of the hybrid global models that use altimeter data in their solutions (CSR3.0, FES 95.2), in contrast to the purely hydrodynamic models (e.g., FES 94.1 [*Le Provost et al.*, 1994]) whose boundaries reach the coast. Even with specially constructed regional models, care must be taken to resolve the reef and island complexes or parameterize them at subgrid scales [*Bode et al.*, 1997]. Here we confine our attention to the more open, yet complex southern entrance to the GBR lagoon (or Capricorn Channel), to demonstrate the use of altimetry to determine sea level variations in a near coast macro-tidal setting.

[6] Some caution is warranted in computing Geostrophic Current Anomalies (GCAs) from the altimetry data in such settings. *Burrage et al.* [1991] have shown that in the GBR region the reef complex enhances "drag" on low frequency flows. Noting that strong tidal currents may act as a "Reynolds stress" on such flows, they modelled this drag in terms of enhanced linearized bottom friction. Recent modelling results (by LBM) suggest this effect results from form drag, as low-frequency flows are diverted by the dense reef matrix. In any case, these nonlinear effects are relatively weak in the more open reef matrix of the central GBR [*Burrage et al.*, 1991], and the momentum balance remains essentially semi-geostrophic away from smaller scale reef structures [*Burrage et al.*, 1994]. Furthermore, as the period of low frequency (subtidal) motion increases, the reef also becomes progressively more transparent to offshelf sea level and current variations [*Burrage et al.*, 1991]. The best approach for deducing near-coastal low frequency current variability may be to employ the high precision altimetric sea level data available from offshore, to help set numerical hydrodynamic model boundary conditions, following the above mentioned approach for constructing regional tidal models. Absolute geostrophic currents deduced from altimetric sea levels at high resolution along model boundaries could be used for this purpose. This will be feasible once enhanced geoids emerge from dedicated satellite gravity missions such as CHAMP and GRACE, launched in July 2000, and March 2002, respectively, and as sufficient data accumulate from close formation flying of TOPEX and JASON. As a first step in that direction, we show that reliable estimates of GCAs can be made on several year timescales at a current meter location on the upper continental slope, provided sufficiently accurate tidal corrections are available. The relatively large angular separation between TOPEX ground tracks ($\sim$3.5°) fails to resolve across-shelf scales. However, by utilizing collinear track analysis, high resolution (order 6 km) can be obtained along track. Hence we avoid conventional bin averaging and 2-D interpolation steps, and instead present the data as along-track profiles.

[7] The main issues we address here are thus: How well do the CSR3.0 tidal corrections perform in the western

Coral Sea and close to the Australian continental margin, and how well do the residual sea levels and computed GCAs compare with low-frequency in situ sea level and current variability? To address these and some related issues, the remainder of the paper is structured as follows: Section 2 describes the characteristic features of the tides in the region. Section 3 compares the tidal models with in situ stations and examines the residuals, which are then correlated with low frequency in situ records in section 4. Section 5 discusses the results, and section 6 forms the conclusions. Appendices (A–C) give details of in situ, altimetric and tidal model data acquisition and processing.

2. Tides of the Coral Sea and Great Barrier Reef

[8] The tides of the Coral Sea and GBR region (Figure 1) exhibit a number of interesting and characteristic features which result from interaction of the tide with the complex topography of the Coral Sea Basin [e.g., *Webb*, 1973a, 1973b; *Amin and Lennon*, 1992], and from additional effects induced by the varying width of continental shelf and the Barrier Reef matrix [*Middleton et al.*, 1984; *Church et al.*, 1985; *Bode*, 1986; *Andrews and Bode*, 1988]. These characteristics provide a challenge, both for tidal modellers and satellite altimetry experts alike, to resolve tidal and low-frequency sea levels and currents with sufficient accuracy and reliability.

[9] Coral Sea tides may be succinctly described by reference to the results of the *Schwiderski* [1980] semi-empirical model or to the purely hydrodynamic FES 94.1 global tidal model of *Le Provost et al.* [1994]. Le Provost et al. found their results compared qualitatively with the original Schwiderski solution. These solutions are characterised by a semi-diurnal wave propagating westward from the central South Pacific through the passage between New Zealand (NZ) and the Solomon Islands. The cotidal map for the dominant semi-diurnal (M2) constituent [*Le Provost et al.*, 1994, Figure 2] shows this wave is influenced to the south, by anti-clockwise phase propagation around NZ, and to the north by clockwise propagation about an amphidrome located in the Solomon Sea. This results in an amplitude maximum exceeding 100 cm at NZ, reducing to 0 cm near Honiara. Amplitudes increase westward to exceed 60 cm along the southern Queensland (Qld) continental slope and in the Gulf of Papua (GOP). The dominant diurnal constituent (K1, their Figure 8), in contrast, shows a simpler structure. Clockwise propagation around an amphidrome located east of NZ results in a northward progression around the East Australian continent in the Tasman and Coral Seas; with amplitudes gradually increasing from 15 cm at New Caledonia, to exceed 30 cm in the north-western Coral Sea and GOP. The tides on the upper continental slope and shelf of the GBR are outside the domain of the *Schwiderski* [1980] model, but are captured in part by the FES95.2 and CSR 3.0 models.

[10] From our harmonic analyses of data from conventional tide gauge and pressure gauge instruments, and from the SF acoustic gauges (see appendix A.1 and B.1 for details), the M2 constituent strongly dominates the 6 other major constituents at the Noumea and Funafuti tide gauges (Figure 3a) and at all the SF sites (Figure 3b except Honiara), and plays a lesser, but still dominant, role at the coastal sites (TV, CF, MR and FR, see Table 1, Figure 2 for locations). The phases for the diurnal (O1, P1, K1) and semi-diurnal (N2, M2, S2, K2) constituents are strongly differentiated, and there is a tendency for semi-diurnal phases to be retarded closer to the Australian coast, consistent with westward propagation of the semi-diurnal wave in this region. This trend is less obvious at the SF sites, with phase at Honiara being more advanced.

[11] Tides on the continental shelf have been observed and modelled numerically by a number of other authors [Andrews and Jeffrey, Large-scale tidal variations along the Great Barrier Reef, unpublished manuscript; *Wolanski and Pickard*, 1985; *Andrews and Bode*, 1988; *Wolanski*, 1994; *Church et al.*, 1985]; a new model spanning the entire GBR domain is under development (by LBM and LB). The tides along the broad continental shelf of the southern GBR [*Bode et al.*, 1997, Figure 19], which is our particular focus, are essentially progressive, with M2 propagating up the Capricorn Channel to the north west between lat 22 and 25 S, with gradual amplification to the west [*Griffin et al.*, 1987]. The tides near Broad Sound (22 S) are anomalously high due to an effect first recognised and explained by the explorer, Mathew Flinders, as recounted by *Middleton et al.* [1984], and *Bode* [1986]. Using linear analytical models *Middleton et al.* [1984] showed that the dense reef matrix seaward of the Sound effectively blocks the tide, with the result that tidal waves penetrating large gaps in the matrix to the north and south converge in the GBR Lagoon and are amplified by a significant factor. Further amplification results from resonant effects, due to the shape and size of Broad Sound. M2 amplitudes increase from approximately 60 cm on the upper continental slope, to exceed 1.5 m along the coast south of Mackay. Experiments with a nonlinear tidal model (by LBM) predict M2 amplitudes of about 2.5 m at the head of the Sound.

[12] Observed M2 amplitudes for the more restricted domain (see rectangle, Figure 2) of the Southern Great Barrier Reef (SGBR) tidal model [*Bode et al.*, 1997] range from 0.5 to 2.5 m with values exceeding 1.3 m occur at Flock Pigeon Island located in Broad Sound, and at Mackay Harbour, Penrith Island and Rosslyn Bay along the central part of the coast (Figure 4).

3. Tidal Model Performance

3.1. Global Tidal Model Intercomparison

[13] Several teams, including representatives of the various tidal modeling groups, have performed comprehensive global tidal model intercomparisons [e.g., *Molines et al.*, 1994; *Shum et al.*, 1997]. These tasks are a major undertaking, especially as existing models are updated and new ones emerge quite frequently. In this study we opted to intercompare a small but representative selection of models to give us an understanding of the model characteristics, errors and differences in implementation and help guide model selection. Here we assess the FES94.1 [*Le Provost et al.*, 1994], Egbert [*Egbert et al.*, 1994], CSR3.0 [*Eanes and Bettadpur*, 1995], CSR2.0 [*Ma et al.*, 1994] and Desai 94.0 [*Desai and Wahr*, 1994] tidal models by comparing the M2 tidal constituent amplitudes and phases obtained from each with harmonic analyses from in situ tide gauges (Table 2). We also implemented FES95.2, which performs similarly to

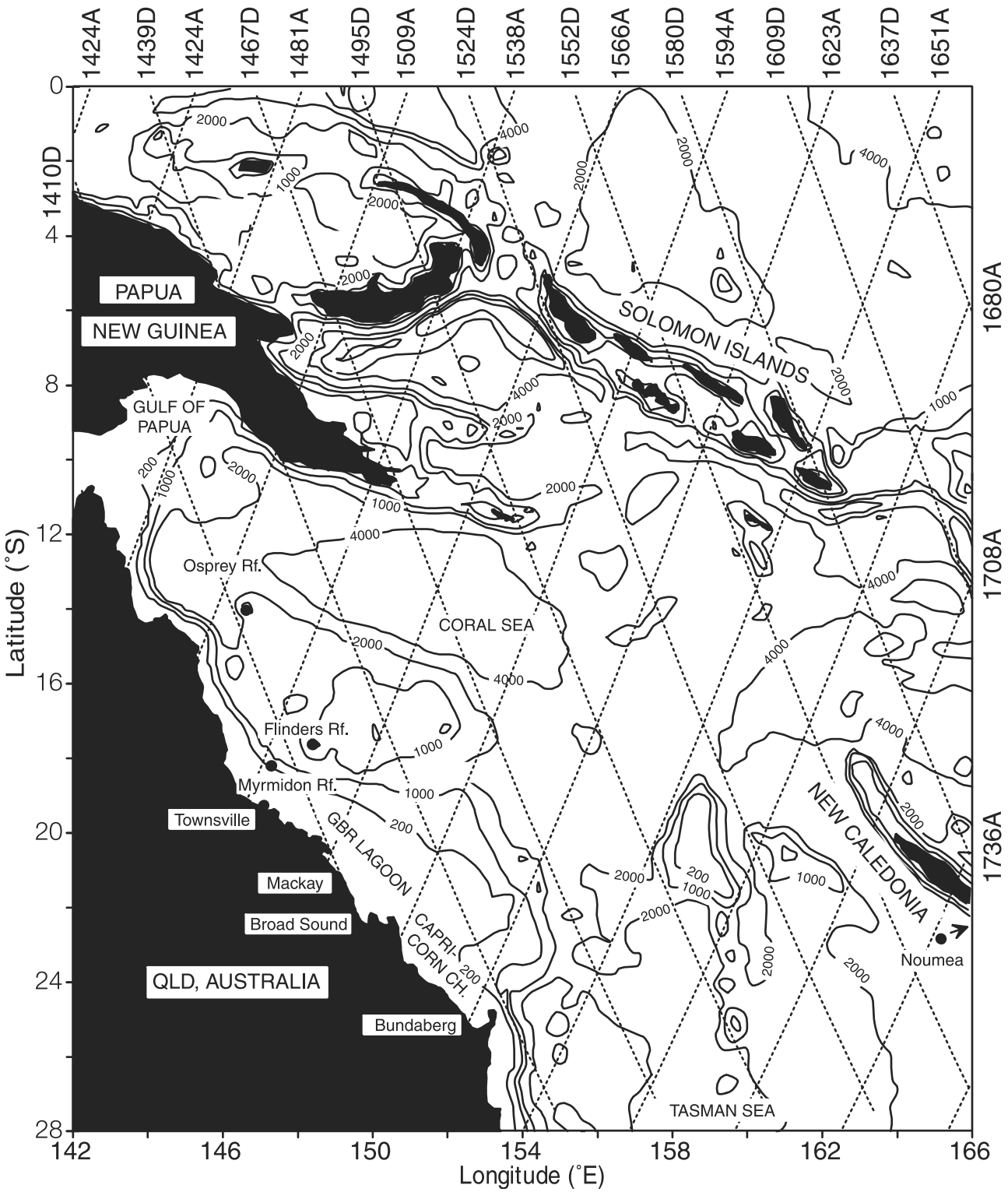

Figure 1. Map showing Coral Sea bathymetry (with isobaths in meters) and locations of TOPEX ground tracks overlaid. Track labels indicate equatorial crossing longitude x 10, and distinguish Ascending (A) and Descending (D) passes. The Great Barrier Reef lies off the Qld coast, inside the 200 m isobath.

CSR 3.0, but have not tested it extensively. Of those we tested, only CSR 3.0 may be considered a ''standard model'' in the sense that it is available on the TOPEX GDRs (along with FES 95.2). CSR3.0 has been widely used by the oceanographic community. However, other models offer improved performance in certain applications. For example, CSR 3.0 has been superseded in some regions by CSR 4.0 and *Foreman et al.* [1998] state that the *Egbert*

Table 1. Locations of Tide Gauges and Current Meter Moorings[a]

Station	Symbol	Lat., dd mm S	Lon., dd nn E
SEAFRAME Acoustic Tide Gauge			
Cape Ferguson, Qld	CF	19 17′	147 03′
Funafuti, Tuvalu	FF(SF)	08 32′	179 13′
Honiara, Solomin Is.	HA	9 26′	159 57′
Lautoka, Fiji	LT	17 36′	177 26′
Port Vila, Vanuatu	PV	17 46′	168 18′
Rosslyn Bay, Qld	RB	23 09′	150 47′
Conventional Tide Gauge			
Bundaberg, Qld	BB	24 50′	152 21′
Noumea, New Caledonia	NA	22 18′	166 26′
Townsville, Qld	TV	19 15′	146 50′
Funafuti, Tuvalu	FT(TG)	8 32′	179 13′
Subsurface Pressure Gauge			
Carter Reef, Qld Shelf	CR	14 32.1′	145 34.1′
Flinders Reef, Qld Plateau	FR	17 42.9′	148 26.8′
Myrmidon Reef, Qld Shelf	MR	18 16.3′	147 22.7′
Osprey Reef, Qld Offshelf	OR	13 52.9′	146 33.5′
Current Meter Mooring			
Jewell Reef	JW	14 20.4′	145 20.5′
Myrmidon Reef	MY	18 13.5′	147 20.9′

[a]Symbols and locations of tide gauges and current meter moorings grouped by installation type. The locations are plotted in Figure 2.

et al. [1994] model has better coverage than CSR 3.0 along the west coast of Canada, while the recently published global tidal model GOT99.2 [*Ray*, 1999] also resolves a number of marginal seas including the Gulf of Maine/Gulf of St. Lawrence on the east coast of the USA and Canada.

[14] Table 2 shows the results of our comparison between the global tidal models and observations from locations in and near the GBR, and around the Coral Sea. For amplitudes, and excluding Noumea, CSR2.0 showed the smallest deviations between the model-predicted and in situ M2 constituent, followed by Desai, CSR3.0 and the purely hydrodynamic FES94.1. With Noumea included, CSR3.0 was better than Desai; FES94 was not considered in this case, since it gave no value for that station. For the phase, excluding Noumea, CSR2.0 clearly performed best, followed by Egbert and CSR3.0, with FES94.1 showing the largest deviations. If Noumea was included, CSR3.0 was the best, followed by Egbert and CSR2.0. Curiously, CSR2.0 generally outperformed CSR3.0, but its spurious phase response at Noumea, presumably due to topographic effects, is a disadvantage. The purely hydrodynamic model FES94.1 was generally less capable than the hybrid models. The models differ in their abilities to resolve islands and other topographic features, so results obtained at such

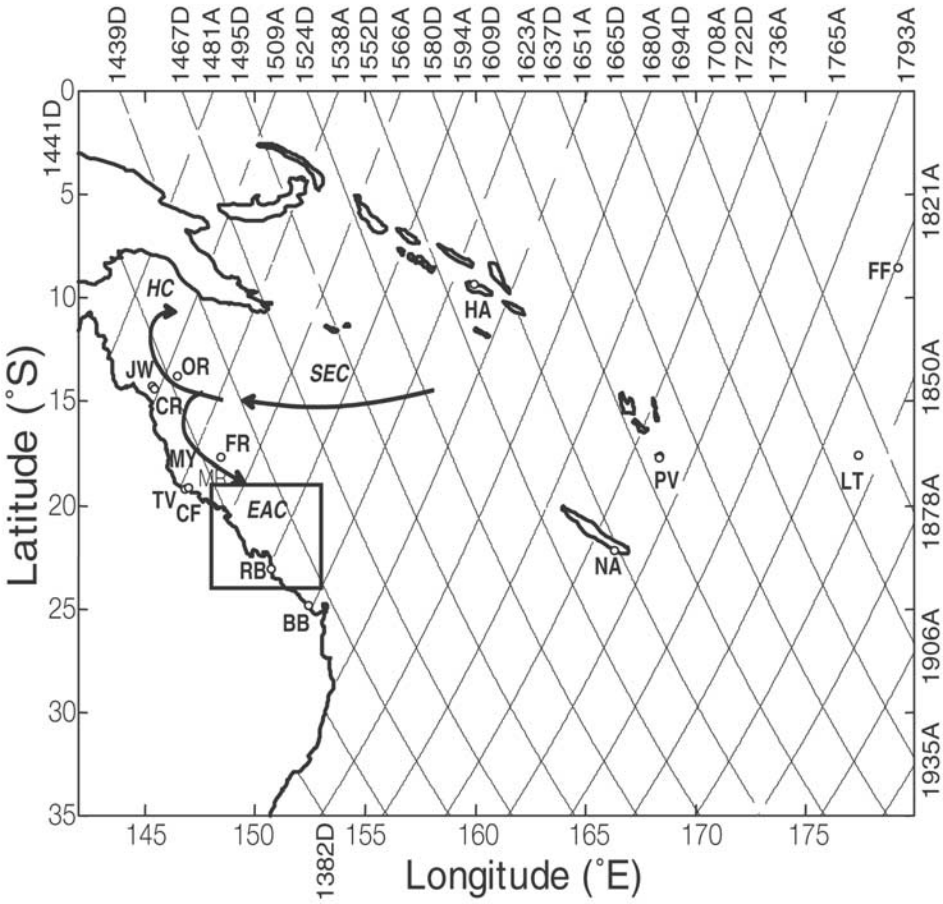

Figure 2. Map showing Coral Sea and western South Pacific to the dateline with Coral Sea circulation scheme and TOPEX ground tracks overlaid. In situ tide gauge and current meter mooring locations are also shown. The rectangle shows the SGBR tidal model domain.

Table 2. Comparison of In Situ M2 Amplitudes and Phases With Predictions From Various Global Tidal Models[a]

Stn	In Situ	FES94.1	Egbert	CSR 3.0	CSR 2.0	Desai
			Amplitude, cm			
TV	73.95	N.A.[b]	N.A.	49.95	58.26	52.23
MR	53.64	60.13	50.12	56.98	55.34	50.99
FR	51.53	55.25	48.58	51.43	51.32	48.64
CR	51.05	54.15	44.61	48.15	49.15	45.61
OR	48.41	53.16	43.27	46.64	48.26	45.35
NA	40.57	N.A.	37.35	38.26	37.1	36.84
FF(TG)	57.37	56.07	55.71	53.54	57.1	57.45
			Greenwich Phase, Degree			
TV	348.7	N.A.	N.A.	346.8	344.2	341.9
MR	341.5	335.4	339.3	338.4	342.7	340.9
FR	339.2	333.7	337.3	343.5	340.9	339.7
CR	346.8	338.8	343.5	343.2	343.2	341.9
OR	343.7	339.1	342.9	343.1	343	342.2
NA	270.2	N.A.	252.3	269.7	244.1	241.9
FF(TG)	154.4	153.7	153.1	154.3	153.8	155.3

[a]Comparison of M2 tidal constituent amplitudes and Greenwich phases obtained from various of the originally proposed TOPEX tidal models (FES94.1, Egbert, CSR3.0, CSR2.0 and Desai) with those from harmonic analyses of the long-term in situ tide gauges at specific locations (see Table 1 for symbol definitions).

[b]Tidal model results are not available for stations marked N.A.

localities are not necessarily indicative of deep ocean model performance.

[15] With no decisive leader among the global tidal models from comparisons with the tide gauge data in the Coral Sea, we decided to proceed with a more detailed assessment of CSR 3.0 (see appendix C for model application details) and the SGBR regional tidal model developed by *Bode et al.* [1997]. CSR 3.0 offers good overall performance at most sites, although there is clearly room for improvement, especially near islands and coasts (the high resolution predictions from the FES95.2 finite element grid might be better, but were not accessible). For work in the Southern GBR region, the Southern GBR Model is a clear choice. Global tidal models either perform poorly or are unavailable for most of this region. It is the only high-resolution numerical hydrodynamic tidal model available for the region, and it allows for the subgrid scale influence of the reef patches using a specially developed reef parameterization scheme [*Bode et al.*, 1997]. This scheme accounts for flow impedance caused by reef patches and separating channels, using a locally parameterized formulation of the momentum balance, embedded within each numerical grid cell. The model code has been successfully applied to several topographically complex tidally dominated regions, e.g., Torres Strait and the Gulf of Papua, *Bode and Mason* [1995]. The model thus offers superior but economical performance in the topographically complex Southern GBR domain.

3.2. Harmonic Analyses and RMS Errors

[16] For CSR 3.0, a total of 22 tidal constituents were available for analysis, while the SGBR model employed 10 major constituents. For the long-term tide gauge data, 149 constituents were analysed, including the mean, Sa and Ssa, monthly and semi-monthly constituents. The major tidal constituents chosen for comparison included 3 diurnal (O1, P1 and K1) and 4 semi-diurnal constituents (N2, M2, S2 and K2).

[17] Constituent amplitudes and phases for the TG and SF stations are shown in Figure 3. The corresponding graph for CSR 3.0 predictions (not shown) was similar, but with the exceptions noted below. For both model predictions and tide gauge records all 7 major constituents exceeded 4.0 cm amplitude, and were larger than the other constituents analysed. The exceptions were the Noumea, K2 and Funafuti, P1 constituents, which were about 3.9 and 2.7 cm, respectively, for the tide gauges and 3.6 and 2.4 cm for CSR3.0. This puts P1 close to the 2N2 (2.2 cm) and MU2 (2.4 cm) values at Funafuti, although it exceeds them at the other stations. The amplitudes and phases from CSR3.0 (including M2), closely approximate those of the tide gauges at all sites except Townsville and nearby Cape Ferguson. Townsville is right at the coastal boundary of CSR 3.0 where the model is relatively inaccurate and the observed M2 amplitudes exceed those of the model by 48%. Amplitude differences for all other stations are less than 7%, with the observed tending to slightly exceed the predicted. Differences between the observed and modelled phases were generally small, even at the coastal station of Townsville.

[18] The results for the M2 constituent for the SGBR model domain also reveal good agreement between the modelled and observed constituents (Figure 4). There is a slight tendency for the model to under-predict the amplitudes at most sites. Exceptions include Wallaby Reef located in the outer reef in the northern part of the model domain and both Mackay Harbour on the coast, and Flock Pigeon Island near Broad Sound, which lie in the central part of the domain. The phases also indicate slight tidal delays in the model relative to observations, with the exception of Wallaby Reef and Abbott Point. These errors are minor, being close to error bounds for most of the analyses.

[19] To provide a more incisive comparison between modelled and observed tidal constituents, we computed the RMS error between the M2 constituent and a combination of all 7 major constituents (A7). This was done by analytically computing the difference sinusoid between the modelled and observed sinusoid for each constituent, taking into account their amplitudes, phases and recognising they have a common frequency. The amplitude of this difference signal divided by $\sqrt{2}$ is the RMS model error, x_i for the constituent i. The total RMS error for A7 is determined concomitantly as, $(\sum x_i^2)^{1/2}$.

[20] Figure 5a shows the CSR3.0 RMS errors for the TG and SF data together. With the marked exception of Townsville and Cape Ferguson, which exceed 15 and 25 cm respectively for M2 and A7, the errors are less than 7 cm. A7 errors range from 2.3 cm at Noumea to 6.5 at Lautoka, while M2 ranges from 0.9 cm at Honiara to 6.0 at Lautoka. Thus in the Coral Sea the total error is largest at Lautoka, followed by Port Vila, Myrmidon, Flinders, Funafuti, Honiara and Noumea, while the order of the last two is reversed for M2. In spite of its higher instrumental precision the SF gauge at Funafuti gives a higher RMS than the conventional tide gauge, perhaps because of the shorter analysis period, combined with the M2 instability noted in Appendix B.1.

[21] Figure 5b shows the corresponding plot for the SGBR model domain, but for M2 only. Here the larger errors in amplitude and phase at Flock Pigeon Island, Penrith Island and Mackay Harbour, which cluster around

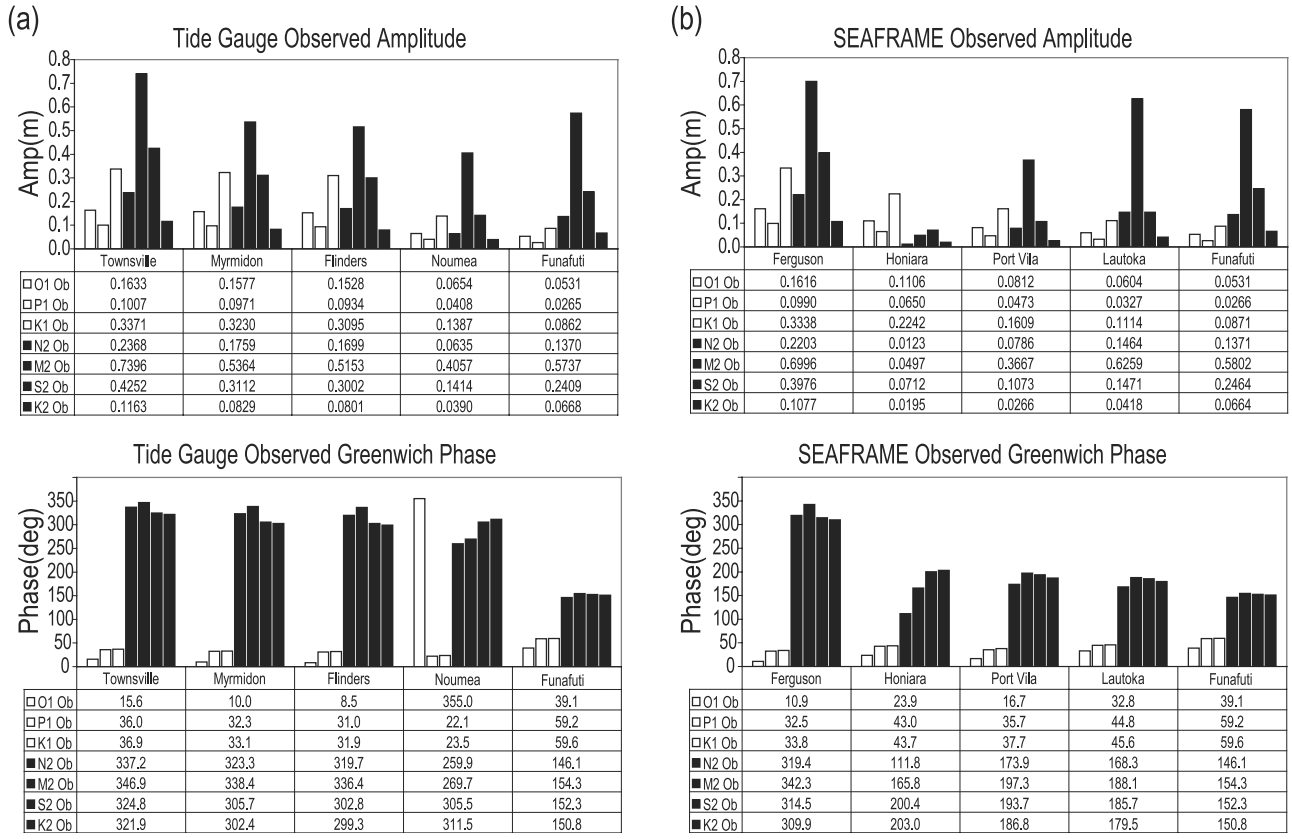

	Townsville	Myrmidon	Flinders	Noumea	Funafuti
O1 Ob	0.1633	0.1577	0.1528	0.0654	0.0531
P1 Ob	0.1007	0.0971	0.0934	0.0408	0.0265
K1 Ob	0.3371	0.3230	0.3095	0.1387	0.0862
N2 Ob	0.2368	0.1759	0.1699	0.0635	0.1370
M2 Ob	0.7396	0.5364	0.5153	0.4057	0.5737
S2 Ob	0.4252	0.3112	0.3002	0.1414	0.2409
K2 Ob	0.1163	0.0829	0.0801	0.0390	0.0668

	Ferguson	Honiara	Port Vila	Lautoka	Funafuti
O1 Ob	0.1616	0.1106	0.0812	0.0604	0.0531
P1 Ob	0.0990	0.0650	0.0473	0.0327	0.0266
K1 Ob	0.3338	0.2242	0.1609	0.1114	0.0871
N2 Ob	0.2203	0.0123	0.0786	0.1464	0.1371
M2 Ob	0.6996	0.0497	0.3667	0.6259	0.5802
S2 Ob	0.3976	0.0712	0.1073	0.1471	0.2464
K2 Ob	0.1077	0.0195	0.0266	0.0418	0.0664

	Townsville	Myrmidon	Flinders	Noumea	Funafuti
O1 Ob	15.6	10.0	8.5	355.0	39.1
P1 Ob	36.0	32.3	31.0	22.1	59.2
K1 Ob	36.9	33.1	31.9	23.5	59.6
N2 Ob	337.2	323.3	319.7	259.9	146.1
M2 Ob	346.9	338.4	336.4	269.7	154.3
S2 Ob	324.8	305.7	302.8	305.5	152.3
K2 Ob	321.9	302.4	299.3	311.5	150.8

	Ferguson	Honiara	Port Vila	Lautoka	Funafuti
O1 Ob	10.9	23.9	16.7	32.8	39.1
P1 Ob	32.5	43.0	35.7	44.8	59.2
K1 Ob	33.8	43.7	37.7	45.6	59.6
N2 Ob	319.4	111.8	173.9	168.3	146.1
M2 Ob	342.3	165.8	197.3	188.1	154.3
S2 Ob	314.5	200.4	193.7	185.7	152.3
K2 Ob	309.9	203.0	186.8	179.5	150.8

Figure 3. Amplitude (m, upper panels) and Greenwich phase (G deg, lower panels) of each of the 7 major constituents at (a) Tide Gauge and (b) SEAFRAME sites. Diurnal and semi-diurnal constituents are shown using white and black bars, respectively. The second semi-diurnal constituent (M2) dominates at all stations except Honiara.

Broad Sound and Mackay (Figure 4), result in M2 RMS errors exceeding 10 cm. At all other stations the error is less than 4 cm, with the minimum occurring at NP2. Errors at the 5 most northerly sites in the GBR lagoon (Wallaby Reef to Creal Reef, inclusive) and at the 2 most southern sites (NP1, NP2) are comfortably under 2 cm, with the exception of Bugatti Reef which exceeds 3 cm.

3.3. RMS Residual SSH

[22] The performance of the global tidal models can also be assessed by examining along-track profiles of RMS residual SSH variability after removal of the tides. The remaining variability can be attributed to unmodelled or poorly modelled (and aliased) tidal variability as well as the spectrum of sea level variability associated with the regional circulation such as wind-driven currents and mesoscale eddies. Figure 6 shows the RMS SSH variability for descending tracks after application of the environmental corrections and tidal correction using CSR3.0. Where the profile rises perpendicularly above the track, RMS variability exceeds 10 cm.

[23] The RMS variability rises from a broad minimum of about 5 cm along lat 20 S to progressively higher levels in the Tasman Sea and generally south of the latitude of New Caledonia. There mesoscale eddies and meanders of the East Australian Current (EAC) and Tasman front might play a role (some of this Tasman Sea variability appears later in the M2 residual tidal alias). The RMS residual generally exceeds 10 cm south of about 23 S. To the north it rises to a modest maximum of 10–12 cm close to 15 S, which lies approximately along the path of the inflowing South Equatorial Current (SEC). It then drops slightly before rising to a broad plateau of about 15 cm around the Solomon Islands. This may be due partly to dropouts, but seasonally varying currents on either side of the archipelago [*Hughes*, 1993] might play a role. Finally, there is an expanse of high RMS variability in a zonal band between 5–10 S lying east of the Solomons between 160 and 170 E. This is not associated with any obvious topographic feature or obstruction, but may be related to the northerly position of the SEC in this region.

[24] The RMS variability is anomalously high off the southern GBR in the latitude range 19 to 25 S. This is largely due to CSR3.0 tidal error associated with the macrotides of Mackay and Broad Sound (21–23 S), and partly due to data dropouts caused by the Great Barrier Reef complex. This anomaly disappears if the SGBR regional tidal model is used to correct the altimetry. Small areas of anomalously high variability appear in the Gulf of Papua (10 S, 145 E), near Noumea, Vanuatu (15 S, 166 E) and in the Solomon Islands (5–10 S, 155–162 E)., There is also evidence of some enhanced sea level variability near the entrance to the Gulf of Papua (12 S, 147 E) and off the Southern PNG Coast (12 S, 148 E), which is influenced by

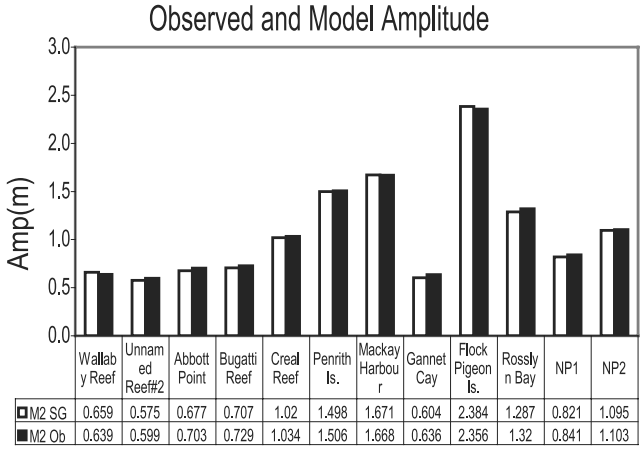

	Wallaby Reef	Unnamed Reef#2	Abbott Point	Bugatti Reef	Creal Reef	Penrith Is.	Mackay Harbour	Gannet Cay	Flock Pigeon Is.	Rosslyn Bay	NP1	NP2
M2 SG	0.659	0.575	0.677	0.707	1.02	1.498	1.671	0.604	2.384	1.287	0.821	1.095
M2 Ob	0.639	0.599	0.703	0.729	1.034	1.506	1.668	0.636	2.356	1.32	0.841	1.103

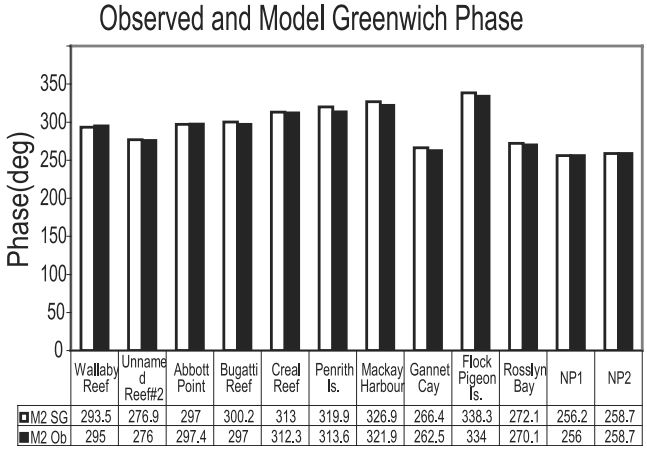

	Wallaby Reef	Unnamed Reef#2	Abbott Point	Bugatti Reef	Creal Reef	Penrith Is.	Mackay Harbour	Gannet Cay	Flock Pigeon Is.	Rosslyn Bay	NP1	NP2
M2 SG	293.5	276.9	297	300.2	313	319.9	326.9	266.4	338.3	272.1	256.2	258.7
M2 Ob	295	276	297.4	297	312.3	313.6	321.9	262.5	334	270.1	256	258.7

Figure 4. M2 Observed (Ob, black bars) and Predicted (SG, white) constituent Amplitude (m, upper panels) and Greenwich phase (G deg, lower panels) at tide gauge sites located within the SGBR model domain. The data are replotted and tabulated from *Bode et al.* [1997 Table 5; Figure 19], which show site locations and co-amplitude and phase contours.

the Hiri Current (HC) [*Burrage*, 1993; *Burrage et al.*, 1995; *Hughes*, 1993]. The overall picture for the Coral Sea is that of moderate RMS variability showing variations consistent with what is known about the general circulation, with larger and sometimes anomalous variability associated either with boundary current variability, or global tidal model errors near coasts, reefs and islands.

[25] The picture for ascending tracks (not shown) is generally consistent with that of the descending tracks (Figure 6). However, the influence of the continental shelf, which widens to the south then narrows suddenly at 23 S is more apparent, and the elevated RMS levels are less obvious in the east central Coral Sea.

[26] The RMS values for descending tracks in the Southern GBR (superimposed in Figure 6) were calculated from altimetry data corrected using the SGBR model. This shows that the large RMS anomaly in the globally corrected data near long 150 E and between 20–25 S is almost entirely removed by use of a high resolution regional tidal model that resolves the reef patches. The ascending track which crosses the GBR, lagoon and coast (not shown) indicates RMS levels rising steadily to about 15 cm near the coast and inside the Lagoon, but with a smaller local peak of about 12 cm crossing the reef complex.

3.4. M2 Alias Errors

[27] We can further assess the tidal models by examining the geographical distribution of the residual tidal errors after correcting SSH using the model. The largest contribution comes from the M2 constituent which has a 62.12 day alias period. We computed this contribution by fitting a pure sinusoid of this period to the residual SSH data after correction using CSR 3.0 (Figure 7). The figure shows along-track profiles of the M2 alias error amplitude for the descending passes through the Coral Sea and GBR region. Profiles rise perpendicularly above the track when the error amplitude exceeds 5 cm. Anomalously large residuals appear along the NE Australian coast, particularly off the southern GBR and along the SW coast of Papua New Guinea. Weaker anomalies (order 5 cm) appear east of New Caledonia. Most of these anomalies are likely due to larger tidal errors near the coast, particularly where the shelf is sufficiently wide to cause amplification. Weak anomalies of 3–5 cm also appear in the Tasman sea and along latitude 33 S, which is close to the location of the eastward branch of the EAC and the Tasman front. These anomalies may be due merely to energetic broadband mesoscale motion appearing at the M2 alias frequency.

[28] The errors are generally modest in the central and northern Coral Sea until the PNG coast and Solomon Island chain is approached. At these locations tidal model errors and data dropouts are expected to degrade the results. However, the Solomon Sea amphidrome likely reduces their impact in that region, while the narrow SE PNG shelf produces little tidal amplification. The same applies to the progressively narrower NE Australian shelf up to a latitude of 13 S, where it broadens into the Gulf of Papua. This suggests that the strong boundary currents over the NE Australian and Southern PNG slope should be amenable to study using altimetry data, adjusted using global (or better still, regional) tidal models.

4. Comparisons of Low Frequency Variability

[29] In the previous section we assessed the performance of CSR3.0 and the SGBR regional model in removing tidal signals from the altimetry data. We now evaluate the low frequency SSH residuals and derived Geostrophic Current Anomalies by correlating them with low frequency sea level and current variations from selected long-term in situ stations.

4.1. Tide Gauge Records

[30] The stations chosen for correlation include all the SF stations (including Rosslyn Bay in the GBR lagoon), a conventional long-term sea level station at Bundaberg, and the TEACS pressure gauge stations Osprey and Flinders Reef (appendix A.1). Only the SF stations may be considered to be accurate and precise over the long-term. The TEACS pressure gauges are subject to drifts in instrument calibration and occasional datum loss, but are useful for correlations on weather band to intraseasonal timescales. To extend their use over interannual timescales, we have

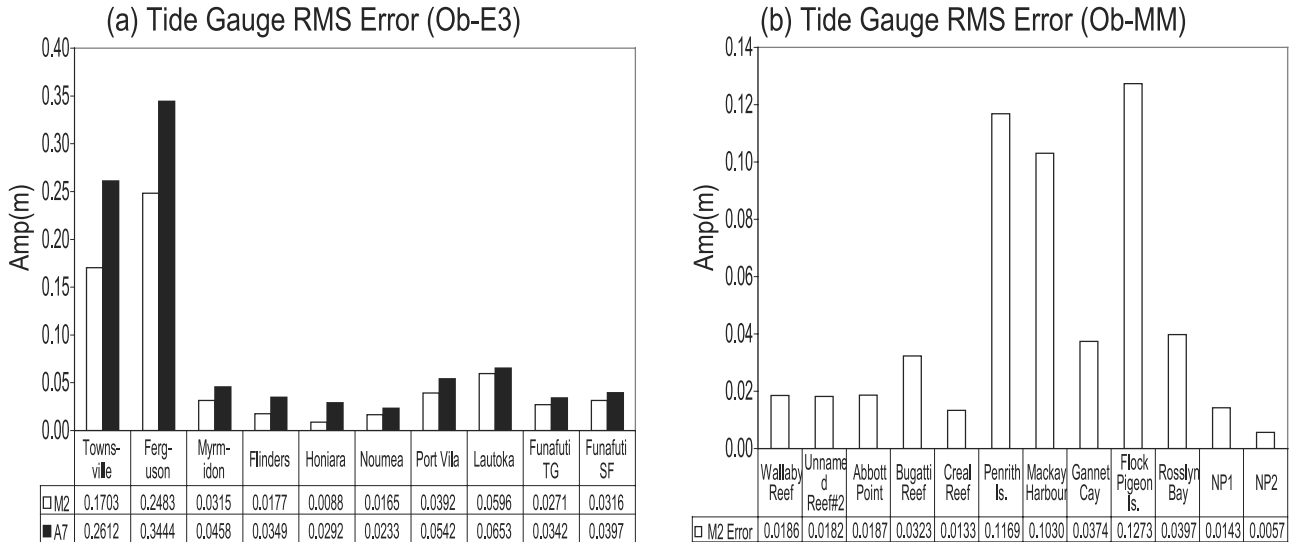

Figure 5. RMS Error for tidal model predictions (observed-model) for (a) CSR 3.0 model showing M2 (white bar) and Total Error (A7, for 7 major constituents, black) at locations spanning the NE Australian continental shelf and the Coral Sea (b) SGBR model showing M2 RMS error only.

applied the corresponding time mean of the TOPEX SSH to adjust the datum of each TEACS data segment.

[31] After smoothing on daily and monthly timescales (appendix B.2), the SSH and in situ data were compared by plotting demeaned time series and their differences, and by computing optimally lagged correlations and linear regressions at specific locations. Means were computed over the full 3.61 yr period of the available TOPEX altimetry record. Representative examples of the corresponding residual time series and regression plots are shown in Figures 8a–8c.

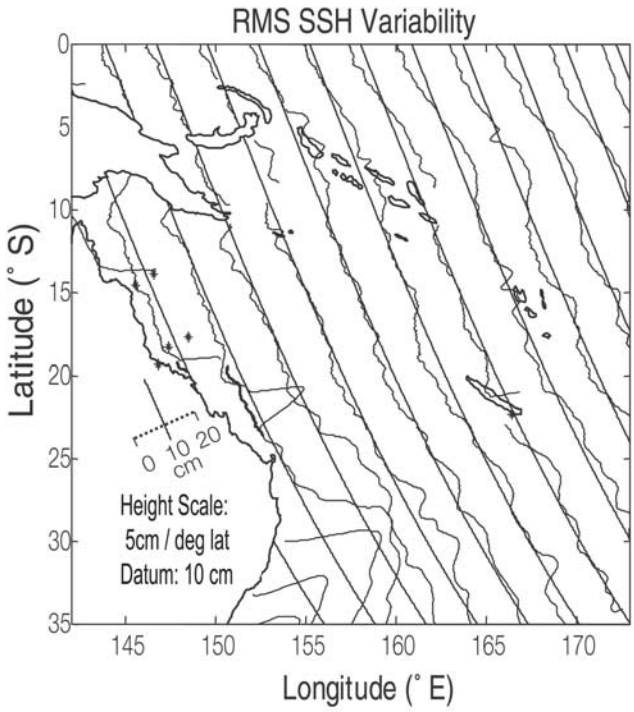

Figure 6. RMS SSH variability after correction using the CSR3.0 global tidal model for descending tracks. The profiles are plotted so that they rise above the corresponding track when the RMS value exceeds 10 cm. RMS SSH variability after correction using the SGBR regional tidal model within its domain is overlaid (bold lines near lat 20 S, 150 E). The intertrack spacing corresponds to a height change of about 17 cm perpendicular to the track (5 cm/deg lat).

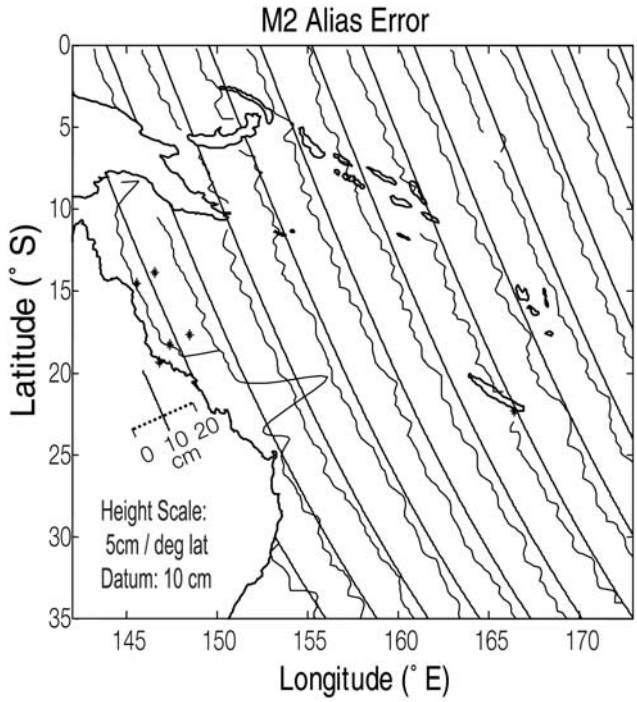

Figure 7. Amplitude of the residual M2 alias for descending tracks through the Coral Sea. The profiles are plotted so that they rise above the corresponding track when the residual M2 alias exceeds 5 cm in amplitude. Height scale factor is the same as for Figure 6.

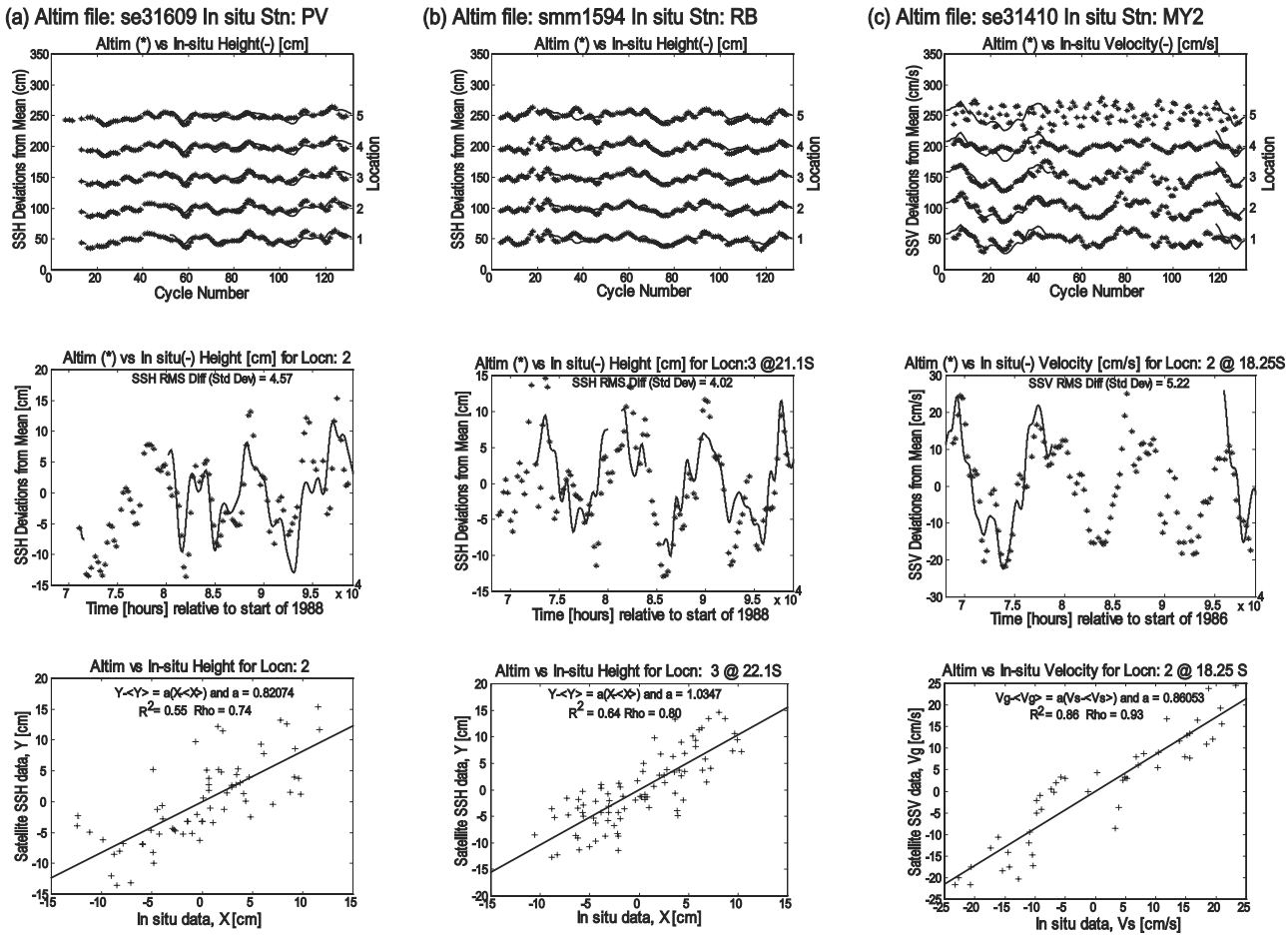

Figure 8. Representative time series and lag correlations for monthly smoothed data. Time series of demeaned in situ (solid) and altimetric (asterisks) data at intervals along track after lag adjustment (top panels). Time series from locations at intervals of (a, c) 0.25 and (b) 0.1 deg of latitude alongtrack are offset along the vertical axes. Time series for the optimal location (center panels). Corresponding lagged regression plot (lower panels). (a) Port Vila and (b) Rosslyn Bay SSH deviations versus de-meaned in situ sea levels. (c) Myrmidon Level 2 de-meaned alongslope (solid) and geostrophic currents (asterisks). High noise levels at location 5 are due to tidal errors and dropouts over the Reef. Results for optimal locations 2, 3 and 2 for PV, RB and MY2, respectively, correspond to entries in Table 3a, Runs 2 and 34, and Table 4, Run 3.

[32] For Port Vila the fit between demeaned altimetry data corrected using CSR3.0 and in situ sea surface height variations remains coherent over a significant latitudinal span (exceeding 1 deg of latitude, Figure 8a, upper panel). The sea level variations, which range over about 20 cm during the observational period, show an RMS difference between the two observational time series of 4.6 cm at location 2 where the fit is best (middle panel). The in situ data explains 55% of the altimeter data variance, while the regression slope coefficient (or ''response factor'') shows that the altimetry fluctuations were attenuated by a factor of 0.8 relative to the in situ fluctuations (lower panel). For observations near Rosslyn Bay, corrected using the SGBR regional tidal model the fit at Location 3 shows fluctuations again ranging over about 20 cm and an RMS difference of 4.0 cm with 64% of the variance explained and no apparent attenuation (Figure 8b).

[33] The lag correlations (or more accurately ''lagged cross-correlations'') were optimized both in space and time. For each of a range of along track locations spaced at regular latitude intervals, the lag time yielding the ''maximum'' value of the correlation coefficient function (or ''normalised cross-covariance function'' of *Bendat and Piersol* [1986, p. 118, equation (5.16)]) was obtained. (When time series that are expected to be negatively correlated are compared, the ''minimum'' correlation should be sought; this can be achieved by reversing the sign of one of the input variables, as we do later for certain current velocity time series.) Corresponding regression relationships (slopes and offsets) were also computed at each location, after adjustment using the lag corresponding to the maximum. The ''optimum'' lagged correlation and corresponding regression relationship were then determined by selecting that location yielding the largest ''maximum'' time-lagged correlation. While the TOPEX data interval is limited to 10 days, the in situ data were sampled hourly. Lags were applied to the smoothed in situ data by advancing or retarding the time by intervals of 1 or more hours, with

Table 3a. Optimal Lagged Correlation of Monthly In Situ Sea Levels and TOPEX SSH[a]

Monthly Run#	Stn	Asc Dsc	Track Posn	Tide Model	Ref_lat., deg	Ref_lon., deg	R_sqrd	Rho	Rms, cms	Ndof Effect.v	Reg_cof cms/cms	Reg#1 Signif.	Tot_dist, km	Opt_lag, hr	Znl_phv, m/s	Mer_phv, m/s	Mer_phv /Rossby
1	FF	A	NW	csr3	−9.45	178.72	0.87	0.93	2.8	18	0.97		116	−17	0.88	1.68	1.94
2	PV	D	XW	csr3	−17.45	167.36	0.55	0.74	4.6	20	0.82		116	−266	0.12	−0.03	−0.15
3	PV	A	XW	csr3	−17.95	166.93	0.46	0.68	4.7	21	0.64	*	163	−84	0.53	0.08	0.37
4	PV	D	XE	csr3	−16.95	169.99	0.7	0.84	4.8	21	1.21	*	214	522	0.10	0.05	0.2
5	PV	A	XE	csr3	−17.45	169.97	0.74	0.86	4.1	22	1.16		196	736	0.07	0.01	0.05
6	LT	A	NE	csr3	−15.20	179.37	0.36	0.60	3.9	32	0.8		349	194	0.32	0.38	1.49
7	LT	A	SE	csr3	−18.95	177.86	0.53	0.73	2.8	25	0.80	*	158	36	0.39	−1.16	−5.62
8	LT	D	NE	csr3	−16.2	178.2	0.56	0.75	2.8	27	0.86		179	−282	−0.09	−0.15	−0.63
9	LT	D	SE	csr3	−18.45	179.10	0.31	0.55	4.0	31	0.74	*	217	−80	−0.68	0.33	1.55
10	LT	A	XW	csr3	−17.95	175.44	0.51	0.71	3.5	32	1.02		236	−69	0.94	0.16	0.72
11	LT	D	XW	csr3	−18.95	176.47	0.54	0.74	3.4	31	1.06		187	−345	0.09	0.12	0.59
12	HA	A	NE	csr3	−6.7	159.88	0.93	0.97	3.1	12	1.20	*	303	69	−0.03	1.22	1.14
13	HA	A	SW	csr3	−9.70	158.78	0.93	0.96	3.5	12	1.22	*	136	69	−0.53	−0.12	−0.16
14	HA	D	SW	csr3	−9.95	158.80	0.89	0.94	3.2	14	1.11		143	−348	0.10	0.05	0.06
15	HA	D	NW	csr3	−5.70	157.24	0.96	0.98	2.9	13	1.25	*	514	146	−0.58	0.79	0.64
16	HA	A	NE	csr3	−8.45	162.08	0.89	0.94	3.2	14	1.13	*	262	−530	−0.13	−0.06	−0.07
17	HA	A	SE	csr3	−10.95	161.15	0.64	0.80	4.8	15	0.72	*	217	31	1.21	−1.52	−2.26
18	HA	D	NE	csr3	−6.70	160.44	0.97	0.98	3.4	12	1.28	*	308	−7	−2.14	−12.02	−11.19
19	HA	D	SE	csr3	−11.95	162.38	0.85	0.92	3.1	10	1.05		392	−2323	−0.03	0.03	0.06
20	BB	A	XW	csr3	−20.15	151.85	0.40	0.63	3.8	17	0.93		525	193	−0.09	0.75	5.56
21	BB	A	XE	csr3	−23.70	153.14	0.29	0.53	4.6	31	0.71	*	156	−1280	−0.02	−0.03	−0.24
22	BB	D	XE	csr3	−24.95	153.58	0.42	0.65	5.0	31	1.07		147	−171	−0.24	0.02	0.19
23	CF	A	XW	csr3	−17.95	147.09	0.47	0.68	4.3	33	0.53	*	148	176	0.01	0.23	1.18
24	CF	D	XE	csr3	−18.95	148.13	0.62	0.79	3.7	33	0.66	*	132	−336	−0.10	−0.03	−0.16
25	CF	A	XE	csr3	−18.70	149.62	0.46	0.68	4.4	32	0.61	*	309	3195	0.03	0.01	0.03
26	OR	A	XW	csr3	−13.95	145.84	0.63	0.80	3.6	18	0.54	*	83	−164	0.14	0.01	0.04
27	OR	D	XW	csr3	−13.20	145.85	0.75	0.87	2.9	19	0.77	*	111	−386	0.06	−0.05	−0.14
28	OR	A	XE	csr3	−14.45	148.48	0.64	0.80	4.6	19	0.80	*	229	169	0.36	−0.10	−0.30
29	OR	D	XE	csr3	−13.95	148.97	0.65	0.81	4.7	17	0.84		276	61	1.26	−0.03	−0.10
30	FR	A	XW	csr3	−17.45	147.29	0.58	0.76	6.1	27	0.41	*	138	−229	0.16	−0.04	−0.16
31	FR	D	XW	csr3	−17.20	147.41	0.53	0.73	6.3	27	0.44	*	133	−504	0.07	−0.03	−0.14
32	FR	A	XE	csr3	−17.95	149.93	0.41	0.64	6.9	26	0.51	*	175	235	0.20	−0.03	−0.14
33	FR	D	XE	csr3	−17.95	150.55	0.62	0.79	5.4	25	0.62	*	247	140	0.49	−0.05	−0.24
34	RB	A	XW	sgbr	−22.05	151.04	0.64	0.80	4.0	26	1.03		126	−188	−0.04	−0.18	−1.35
35	RB	D	XE	sgbr	−22.55	152.50	0.45	0.67	4.7	26	0.83		217	25	2.30	0.74	5.68
36	RB	A	XE	csr3	−23.95	153.03	0.32	0.57	4.8	26	0.60	*	286	−21	−3.60	1.18	9.60
37	RB	A	XW	csr3	−19.55	152.10	0.23	0.48	5.1	30	0.46	*	430	3145	0.01	0.04	0.24
38	RB	D	XE	csr3	−25.05	153.62	0.46	0.68	5.0	26	0.88		405	−213	−0.45	0.28	2.36

[a]Comparison of monthly smoothed in situ sea level and altimetric SSH data using optimal lagged correlation. The columns include a run sequence number, station label, flag for ascending (A) or descending (D) tracks and relative track location. The last is shown as W or E depending on whether the track passes west or east of the station, N or S where track data is interrupted near the station and correlated with points either north or south along track (or X if the track data are uninterrupted). The tide model is either CSR 3.0 or SGBR. Track latitude and longitude give the optimal lag point location on the track. The succeeding statistics are the correlation coefficient, Rho, the root mean square of the regression residuals, Rms, the effective number of degrees of freedom (allowing for autocorrelation due to smoothing), the regression coefficient, and a flag (asterisk) indicating when this is significantly different from unity. There follows the total distance between station and optimal lag point, the corresponding optimum lag, zonal and meridional phase velocity, and finally the meridional phase velocity normalized by the corresponding Rossby wave phase speed. All correlations were significant at the 95% level.

respect to the TOPEX cycle time base, before decimating them to 10 day intervals. Latitude intervals for lag correlation were 0.25 deg (27.8 km) for data corrected with the CSR3.0 tidal model (filter cutoff wavelength 36 km). Intervals of 0.1 deg (11 km) were used for data corrected using the SGBR model (cutoff wavelength 18 km). Hence in both cases, the spatial intervals were slightly oversampled with respect to the filter cutoff wavelength.

[34] The optimal lag locations and corresponding correlation coefficients (Rho) and linear regression coefficients for each site with its adjoining ascending and descending tracks were tabulated (Table 3) along with several related statistics. These include inter alia the effective number of degrees of freedom, allowing for autocorrelation induced by the time domain filters, and the direction and speed of propagation (phase velocity) derived from the optimum lags (distance of optimal lag location along-track to in situ station divided by the lag time). Both meridional and zonal components of phase velocity were determined. These were subsequently normalised by the Rossby wave speed for the relevant latitude to facilitate interpretation, particularly at the open ocean sites, where planetary Rossby wave dynamics might be expected to dominate the circulation.

[35] A plot summarising all the optimal lag correlations for the monthly smoothed data for all stations is shown in Figure 9. Stations in the western Coral Sea and GBR region in order moving northward at or near the NE Australian coast are BB, RB, CF, FR and OR, respectively. Those in the central and eastern Coral Sea are in order eastward HA, PV, LT and FF. We now examine the correlations in these two areas.

4.1.1. Central and Eastern Coral Sea

[36] Of the stations in the central and eastern Coral Sea, HA and FF show particularly high correlation values, while intermediate values appear at PV and LT. The high correlation at HA is related to the M2 tidal amphidrome lying in this region (Figure 3b), which reduces residual tidal errors (Figure 5a). Lags at PV show consistently eastward phase propagation while those at FF and LT show a preference for

Table 3b. Optimal Lagged Correlation of Daily In Situ Sea Levels and TOPEX SSH[a]

Daily Run#	Stn	Asc Dsc	Track Posn	Tide Model	Ref_lat, deg	Ref_lon, deg	R_sqrd	Rho	Rms, cms	Ndof Effect.	Reg_cof cms/cms	Reg#1 Signif.	Tot_dist, km	Opt_lag, hr	Znl_phv, m/s	Mer_phv, m/s	Mer_phv /Rossby
1	FF	A	NW	csr3	−9.45	178.72	0.75	0.87	4.3	63	0.95		116	−104	0.14	0.27	0.32
2	PV	D	XW	csr3	−17.45	167.36	0.45	0.67	6.8	66	0.89		116	−375	0.08	−0.02	−0.10
3	PV	A	XW	csr3	−17.45	167.14	0.41	0.64	7.2	48	1.03		141	−376	0.10	−0.02	−0.10
4	PV	D	XE	csr3	−16.95	169.99	0.53	0.73	7.2	68	1.03		214	325	0.17	0.07	0.32
5	PV	A	XE	csr3	−17.45	169.97	0.62	0.79	6.5	67	1.20		196	519	0.10	0.02	0.08
6	LT	A	NE	csr3	−15.20	179.37	0.24	0.49	6.0	103	0.66	*	349	175	0.36	0.42	1.65
7	LT	A	SE	csr3	−18.95	177.86	0.34	0.58	4.5	69	0.72	*	158	42	0.33	−0.99	−4.82
8	LT	D	NE	csr3	−16.20	178.20	0.47	0.68	3.9	75	0.89		179	−379	−0.06	−0.11	−0.47
9	LT	D	SE	csr3	−18.70	179.21	0.26	0.51	6.0	91	0.68	*	241	127	0.45	−0.27	−1.28
10	LT	A	XW	csr3	−17.95	175.44	0.29	0.53	5.9	104	0.76	*	236	9	−7.19	−1.20	−5.51
11	LT	D	XW	csr3	−18.70	176.37	0.28	0.53	5.6	102	0.74	*	174	−363	0.10	0.09	0.45
12	HA	A	NW	csr3	−6.95	159.79	0.85	0.92	4.8	31	1.23	*	276	−59	0.09	−1.30	−1.24
13	HA	A	SW	csr3	−9.70	158.78	0.88	0.94	5.4	31	1.36	*	136	17	−2.16	−0.50	−0.65
14	HA	D	SW	csr3	−8.95	158.43	0.86	0.93	7.9	32	1.69	*	180	−232	0.21	−0.06	−0.08
15	HA	D	NW	csr3	−6.45	157.51	0.91	0.95	3.5	27	1.15	*	430	−121	0.63	−0.76	−0.68
16	HA	A	NE	csr3	−8.70	161.99	0.83	0.91	4.5	46	1.06		242	66	0.96	0.34	0.40
17	HA	A	SE	csr3	−10.95	161.15	0.70	0.84	4.7	42	0.80	*	217	47	0.80	−1.00	−1.49
18	HA	D	NE	csr3	−6.70	160.44	0.85	0.92	5.9	36	1.28	*	308	−41	−0.37	−2.05	−1.91
19	HA	D	SE	csr3	−11.20	162.10	0.84	0.92	3.3	17	0.89		312	−277	−0.24	0.20	0.30
20	BB	A	XW	csr3	−20.25	151.81	0.22	0.47	7.0	43	0.47	*	514	−40	0.48	−3.54	−26.38
21	BB	A	XE	csr3	−24.05	152.98	0.18	0.42	9.4	107	0.59	*	114	−11	−1.86	−2.20	−19.37
22	BB	D	XE	csr3	−24.70	153.46	0.41	0.64	8.3	101	0.87		133	−245	−0.15	−0.02	−0.15
23	CF	A	XW	csr3	−18.20	146.99	0.36	0.60	8.3	94	0.55	*	121	−35	0.06	−0.96	−4.88
24	CF	D	XE	csr3	−18.95	148.13	0.41	0.64	8.0	98	0.55	*	132	−248	−0.14	−0.04	−0.22
25	CF	A	XE	csr3	−19.45	149.31	0.23	0.48	11.3	68	0.55	*	267	20	3.70	−0.26	−1.41
26	OR	A	XW	csr3	−13.45	146.03	0.53	0.73	5.2	83	0.83		77	−226	0.07	−0.06	−0.16
27	OR	D	XW	csr3	−13.45	145.94	0.47	0.69	5.3	77	0.70	*	85	−438	0.04	−0.03	−0.08
28	OR	A	XE	csr3	−13.95	148.68	0.53	0.73	6.5	78	0.89		243	247	0.27	−0.01	−0.02
29	OR	D	XE	csr3	−13.95	148.97	0.46	0.68	6.9	67	0.76	*	276	−227	−0.34	0.01	0.03
30	FR	A	XW	csr3	−17.45	147.29	0.26	0.51	8.6	89	0.35	*	138	−9	4.15	−0.91	−4.09
31	FR	D	XW	csr3	−17.45	147.52	0.30	0.55	7.9	91	0.39	*	112	−229	0.13	−0.04	−0.16
32	FR	A	XE	csr3	−17.70	150.03	0.21	0.46	8.8	91	0.44	*	185	444	0.12	0.00	0.00
33	FR	D	XE	csr3	−17.95	150.55	0.41	0.64	7.7	84	0.53	*	247	363	0.19	−0.02	−0.09
34	RB	A	XW	sgbr	−22.25	150.95	0.42	0.64	9.0	64	0.77		102	−229	−0.02	−0.12	−0.92
35	RB	D	XE	sgbr	−22.15	152.32	0.41	0.64	8.1	90	0.49	*	216	−241	−0.21	−0.13	−0.96
36	RB	A	XE	csr3	−24.05	152.98	0.10	0.32	10.3	88	0.36	*	285	−14	−5.29	1.99	16.27
37	RB	A	XW	csr3	−19.95	151.93	0.12	0.35	8.4	91	0.26	*	381	85	0.45	1.16	7.90
38	RB	D	XE	csr3	−24.65	153.44	0.38	0.62	9.3	91	0.61	*	364	−248	−0.36	0.19	1.57

[a]Comparison of daily smoothed in situ sea level and altimetric SSH data using optimal lagged correlation. See Table 3a footnote for notation details.

phase propagating toward the in situ station. This effect could result from local topographically induced delays in the penetration of sea level anomalies. The lag results for HA are mixed. The larger lags place the in situ response later than the corresponding SSH signal at the optimal lag location on the TOPEX ground track. However, there is also an indication of northward and westward phase propagation at the site. For the daily smoothed data (Table 3b), the results are generally consistent with those of Table 3a, as shown in Figure 9, but the correlations are slightly weaker. The lag results are also similar, but with stronger preference for HA to lag the SSH, suggesting this effect is related to the shorter low-frequency timescales.

[37] Some of the lags appear unrealistically large (∼1000 hours) and approach seasonal timescales. This might result from large-scale quasi-stationary or very slowly evolving circulation features which would be excluded by potential vorticity conservation from entering reef and island chains intact, but might indirectly influence sea levels at the in situ station through local momentum and mass exchange processes. To give an indication of the actual phase propagation speed (compensating the lags for the effect of distance from the station), we also compute the phase velocities (Figure 10). These are presented as vectors with the same sense of propagation direction as the lags in Figure 9.

[38] Figure 10 also shows the response factors (Slp) of SSH versus the in situ sea level variations for all stations for the monthly data. The corresponding daily data follow a similar pattern, but are more variable (Table 3b). The results show that the sea level changes at HA are slightly attenuated relative to the satellite-derived values. In contrast the values at LT tend to be amplified. The response factor at FF is apparently near unity, while PV shows a tendency for SSH to be attenuated in the west and amplified in the east, relative to the in situ station. This suggests sea level anomalies grow in intensity as they propagate eastward through the Vanuatu island chain.

4.1.2. Western Coral Sea

[39] Correlations for the western Coral Sea stations are comparable with those at PV and LT, discussed above (Figure 9). For the monthly smoothed data, phase propagation is consistently eastward and southward at OR and FR. The coastal site, CF, tends to lag SSH on the shelf and lead it in the deeper water, which suggests the dominant sea level anomalies originate on the outer shelf or slope, perhaps as a result of coastal-trapped waves.

[40] A similar pattern in the phase propagation applies to RB and BB which show shoreward propagation near the coast and inside the GBR Lagoon, and a tendency for offshore propagation at off shelf locations. These can be

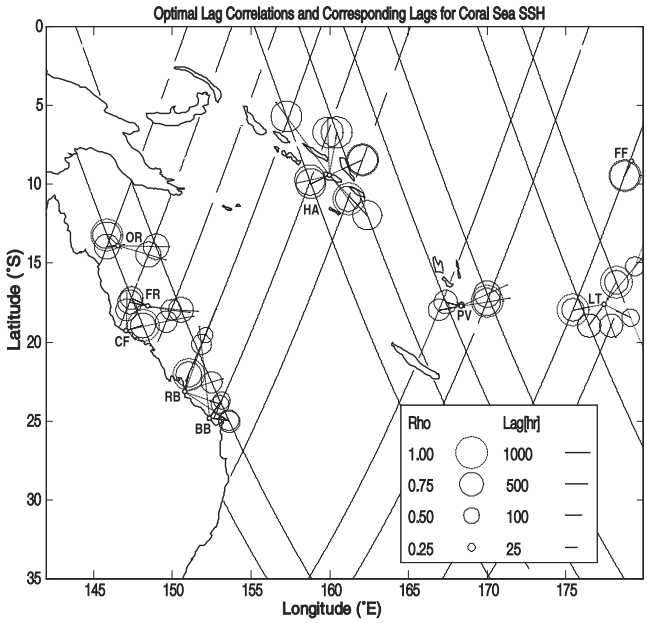

Figure 9. Optimal lag correlations for all stations examined for monthly smoothed data. All correlations shown in this and the subsequent figs are significant at the 95% level. Radii of the solid circles represent the correlation coefficient; ideal Rho = 1.0 circles (dashed) are included for comparison. Corresponding lags are indicated by the lines emanating from circle centres that point in the direction of phase propagation (either away from or toward the in situ station according as the SSH data lags or leads the in situ station). Line length is scaled by log10 of actual lag value, but actual values appear in the legend labels (not the exponent). The centre of each circle lies at the point of optimal lagged correlation along the relevant descending or ascending TOPEX ground track.

seen more clearly in relation to the topographic details of the GBR in Figures 11 and 12. Data from the ascending and descending tracks passing either side of RB were corrected using the SGBR tidal model, while those east of BB, which is outside the SGBR model domain, were corrected using CSR3.0.

[41] The correlations with RB and BB from nearby track locations are modest to high, with lower correlations off shelf. The correlation with RB (0.80) at one location in the outer lagoon (near 22 S,151 E, Table 3a, Run#34) is also surprisingly high, which suggests the Lagoon responds coherently at low frequencies. At this location the correlation with the daily smoothed data is also high (0.77). This high correlation appears in a topographically complex domain which involves strong forcing by the EAC and a strong interplay between synoptic, mesoscale and submesocale circulation processes [*Burrage et al.*, 1996].

[42] The response factors for the western sites (Figure 10) all have a tendency for the sea level variability to be higher at the in situ station than along the TOPEX ground tracks, particularly for the continental shelf sites (e.g., RB, Figure 12) where coastal trapped waves might play a role. This effect is especially marked for the daily smoothed data (Table 3b) which includes the weather band.

4.2. Current Meter Records

[43] Time series of GCAs were computed for locations on TOPEX ground tracks and compared with the alongslope current component from the nearby current meter moorings (appendix A.2). These observations are strongly influenced by the northward (HC) and southward (EAC) branches of the SEC, which flows into the Coral Sea primarily between the Solomon Islands and New Caledonia [*Andrews and Clegg*, 1989]. Across-track GCAs were computed from the along-track gradients of monthly smoothed and tidally corrected SSH data, with no subsequent filtering. The tracks analysed were the ascending and descending tracks closest to the current meter site. Thus the two current vectors were not necessarily optimally aligned along the flow, and in the absence of shear or other flow inhomogeneities, should scale as the cosine of the angle between them.

[44] The currents from the moorings were compared with the TOPEX GCAs using optimal lagged correlation analysis, as for the sea level data. For the in situ currents, the along-slope components were used because the moorings are close to a steep continental margin and currents are thus constrained by the topography. Furthermore, only the along-slope currents are expected to be in geostrophic balance, as the momentum balance is semi-geostrophic [*Burrage et al.*, 1991].

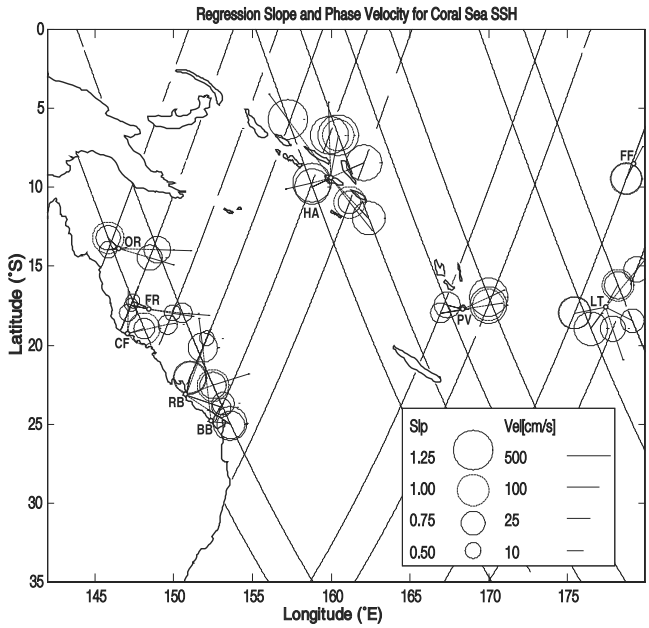

Figure 10. Regression coefficients (slopes) of SSH versus the in situ sea level variations for all stations for the monthly smoothed data. The coefficient values (solid circle radii) at each optimal lag location may be compared with the ideal value of unity (dashed circles). Where the indicated coefficient value exceeds (is less than) unity, the SSH fluctuations exceed (are less than) the corresponding in situ fluctuations, implying the in situ station response is attenuated (amplified). Lines emanating from circle centres represent the total phase velocity as computed from the lags in Figure 9 and distance from station. These lines, with lengths scaled by log10 also point in the direction of phase propagation.

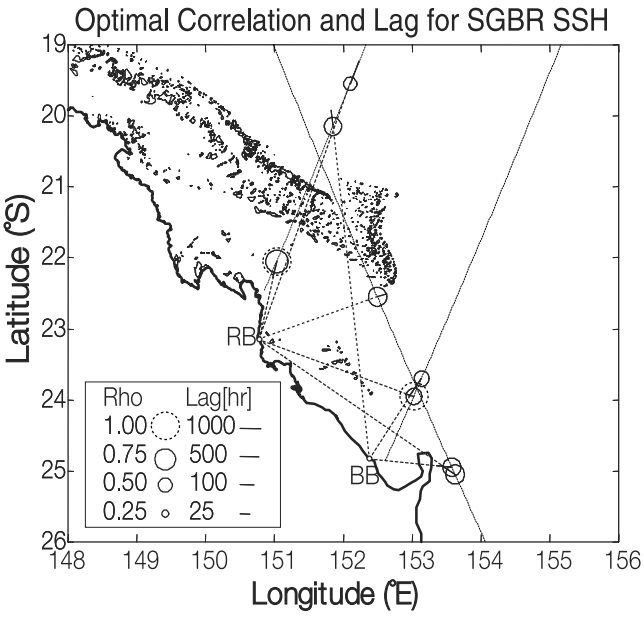

Figure 11. Optimal lag correlations for stations in the Southern GBR for monthly smoothed data. The data partly duplicates that in Figure 9, but the relationship with the Great Barrier Reef topography is revealed. Data from the tracks passing either side of RB were corrected using the SGBR tidal model; those east of BB were corrected using CSR3.0. (See Figure 9 caption for notation details.)

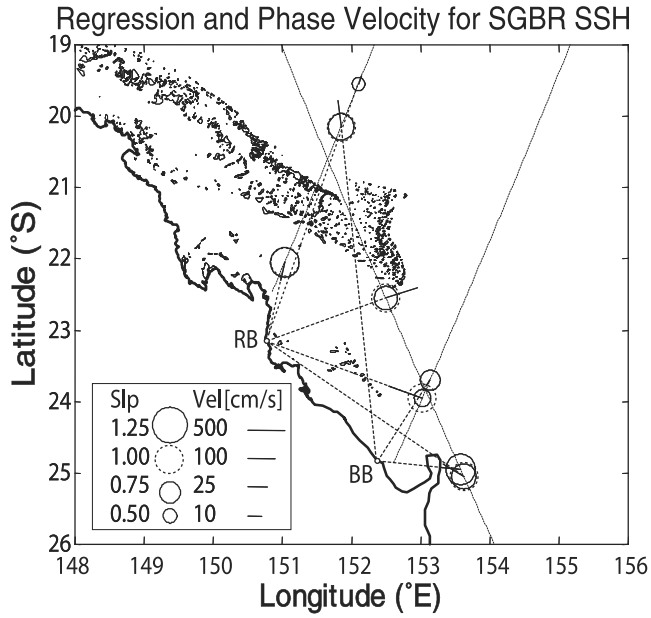

Figure 12. Regression coefficients (duplicating data in Figure 10) for stations in the Southern GBR. See Figure 10 caption for annotation details.

[45] Optimal lag correlations (Table 4, Figure 13) were computed between GCAs and the along-slope component of current over a range of along-track locations. Figure 8c shows an example run which is for MY2 along slope currents. The correlation circles for the different depth levels, which are at optimal lag locations along ground tracks, are closely coincident, or at least overlapping, at each mooring. Correlations are consistently high (>0.7) and significant at the 95% level at Myrmidon, and phase propagation directions scatter about the along-slope direction. They were lower at the Jewell Reef mooring and below the significance level in two cases (Table 4). All in situ time series were initially sign reversed (multiplied by −1, as indicated in col 2) to invert the phase relationship between the positive eastward GCAs from the SSH data, and the positive northward along-slope current observations, to match the prevailing current flow directions of the SEC, EAC and HC (sign reversal is necessary for anticorrelated signals because our software seeks only maximum, not minimum, cross correlation values). Signs were reversed for the Myrmidon mooring because eastward (+ve) flow across the ground tracks is consistent with poleward (−ve) flow in the EAC current at the mooring. They were reversed at Jewell because westward (−ve) SEC inflow crossing the ground tracks is consistent with equatorward (+ve) flow in the Hiri Current. The latter assumes the SEC bifurcation lies south of the mooring, which according to the direction of the TEACS current meter time series, is

Table 4. Optimal Lagged Correlation of Monthly In Situ and TOPEX Geostrophic Current Anomalies[a]

Monthly Run#	Stn	Asc Dsc	Track Posn	Ref_lat, deg	Ref_lon, deg	R_sqrd	Rho	Rms, cms	Rho Signif.	Ndof Effect.v	Reg_cof cms/cms	Reg#1 Signif.	Tot_dist, km	Opt_lag, hr	Znl_phv, m/s	Mer_phv, m/s	Mer_phv /Rossby
1	MY1(−1)	D	XE	−18.45	147.92	0.61	0.78	9.1	*	18	0.65	*	72	−150	−0.12	0.05	−0.23
2	MY1(−1)	A	XW	−17.45	147.29	0.67	0.82	8.6	*	18	0.70	*	86	−110	0.02	−0.22	1.03
3	MY2(−1)	D	XE	−18.20	147.82	0.85	0.92	5.2	*	14	0.86	*	55	−305	−0.05	0.00	0.01
4	MY2(−1)	A	XW	−17.95	147.09	0.73	0.86	8.4	*	14	1.00		43	10	−0.83	0.85	−4.02
5	MY3(−1)	D	XE	−18.45	147.92	0.51	0.71	8.6	*	19	0.90		72	−45	−0.42	0.15	−0.75
6	MY3(−1)	A	XW	−17.95	147.09	0.59	0.77	9.0	*	19	1.10		43	−285	0.03	−0.03	0.14
7	MY4(−1)	D	XE	−18.45	147.92	0.74	0.86	8.0	*	14	1.51	*	72	−10	−1.87	0.69	−3.39
8	MY4(−1)	A	XW	−17.95	147.09	0.63	0.79	6.9	*	14	1.14		43	340	−0.02	0.03	−0.12
9	JW1(−1)	D	XE	−14.20	146.23	0.11	0.33	9.6		19	0.23	*	103	1435	0.02	0.00	0.01
10	JW1	D	XE	−14.95	146.52	0.44	0.67	8.0	*	19	0.59	*	152	−705	−0.05	0.03	0.08
11	JW1(−1)	A	XE	−14.45	145.65	0.35	0.59	25.8	*	18	1.91	*	37	1540	0.01	0.00	−0.01
12	JW2(−1)	D	XE	−14.70	146.43	0.10	0.32	9.6		15	0.28	*	131	−3455	−0.01	0.00	0.01
13	JW2	D	XE	−15.45	146.72	0.25	0.50	8.2	*	17	0.40	*	201	−1425	−0.03	0.02	0.08
14	JW2(−1)	A	XE	−14.20	145.74	0.27	0.52	35.0	*	18	2.32	*	49	830	0.02	0.01	0.02

[a]Comparison of in situ current meter and altimetry-derived GCAs for monthly smoothed data. Column definitions are the same as for Table 3a (see footnote) except that correlations which are statistically significant at the 95% level are explicitly flagged (Rho Sig), the Tide Model is omitted since CSR 3.0 was used throughout. Station symbols refer to Myrmidon (MY) depth levels 1–4 and Jewell Reef (JW) levels 1–2, respectively; the (−1) indicates sign reversal (see text for details).

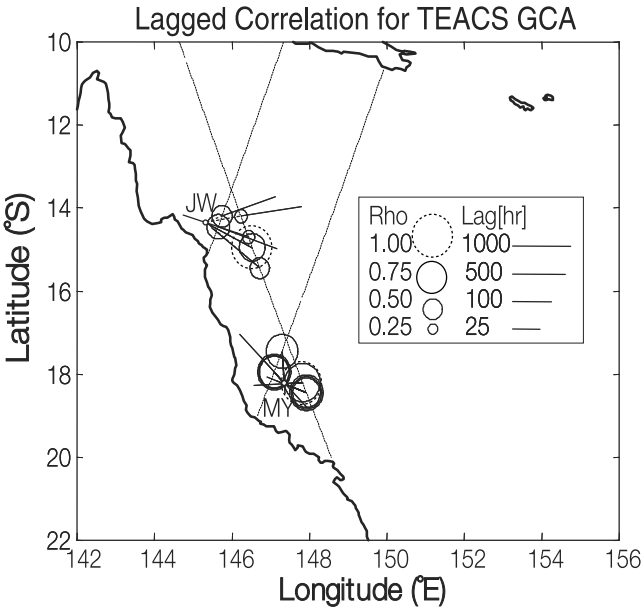

Figure 13. Optimal lag correlations between observed along slope currents and GCAs for monthly smoothed data at the moorings off Jewell and Myrmidon Reefs. Correlation circles from different depth levels are superimposed at their respective optimal lag locations. See Figure 9 caption for other annotation details.

normally the case (D. M. Burrage, and C. R. Steinberg, Transports of the East Australian Current System (TEACS): A decadal scale time series of currents and sea levels from the NE Australian continental margin, manuscript submitted to *Journal of Geophysical Research*, 2003, hereinafter referred to as B&S). However, reversals may occur which occasionally place the mooring in the Southern (EAC) branch of the bifurcation. To test whether southward flow might predominate, we performed correlations with no sign reversal at Jewell Reef and found, somewhat surprisingly, that these correlations were statistically significant and either higher than (shallower JW1) or comparable to (deeper JW2) the sign-reversed case. There are a number of possible explanations for this result (see below), but the most obvious is that the mean bifurcation position might have been located north of Jewell Reef for the particular period of the available TOPEX and Jewell Reef records.

[46] The generally better correlation at Myrmidon Reef than at Jewell has several possible explanations: The southern boundary current branch (EAC) has a broader, more coherent and positionally invariant flow than the northern branch (HC), since the SEC bifurcation at near surface levels lies close to the Jewell Reef mooring and may change its position on seasonal and interannual timescales [B&S, *Burrage et al.*, 1995, *Hughes*, 1993]. Indeed, time series of the GCAs and in situ currents from Jewell Reef (not shown) confirm that the two time series fluctuate in phase for quite long periods then shift out of phase, presumably as the bifiurcation point moves past the mooring location. One of us (LBM) has also found indications from numerical hydrodynamic modelling experiments (supported qualitatively by shipboard Acoustic Doppler Current Profiler observations [*Hughes*, 1993]) that during strong northward flow events the boundary current may separate from the reef edge, which lies only about 1 km from the mooring, while it tends to remain attached during southward flow. We thus suspect the HC separates inertially from the reef edge as the latter bends to the west upstream of the mooring. In this case the JW mooring data would be biased against northward flow. In contrast the Myrmidon current mooring is located further seaward of the reef on a more gentle slope and it is directly and perennially exposed to the EAC flow (although strong SE trade wind events and shelfbreak eddies occasionally cause significant horizontal shear and can even reverse the direction of the near-surface current). Other factors that might influence the reliability of the correlation at Jewell Reef include noise in the altimetry data close to the reef edge, and the possibility that the momentum balance might be ageostrophic near where the bifurcation intersects the shelf break.

[47] While the correlations for the ascending track are statistically significant and comparable with those of the descending track, the RMS residual levels are much higher for the ascending case (Table 4). This is probably a consequence of the CSR3.0 failing to give good tidal corrections near the reef edge (Figure 8c, Location #5 reveals such errors). A newly constructed tidal model which extends the regional tidal model into this part of the continental margin should resolve this issue. The lagged correlations for the Myrmidon current meter mooring are also generally higher than those obtained for the various sea level intercomparisons. This might partly be explained by the computed SSH gradients being less sensitive to tidal errors than the SSH itself, since the tides vary only gradually in space, but rather rapidly in time. The tidal error is effectively filtered out by the differentiation process, since cycle to cycle changes in spatial mean sea levels have no effect on the gradients. It may also result from the closer proximity of this mooring to the TOPEX ground tracks than that of the other in situ stations.

5. Discussion

[48] Performance comparisons of various global tidal models for correcting TOPEX altimetry in the Coral Sea revealed no clearly outstanding candidate, although the ''Standard'' CSR3.0 model offers effective overall performance, and is readily accessed and applied. In general the appropriate choice of global or regional model depends upon the desired application and resolution, and is affected by the relative mix of deep ocean, continental shelf or reef and island topography in the study domain.

[49] We assessed tidal model performance in a number of ways, each of which has strengths and weaknesses. Comparisons of predicted and observed tidal constituent amplitudes and phases using harmonic analysis provides a test that is obviously independent of the TOPEX altimetry data, except to the extent that the altimetry is assimilated into the model, as in CSR 3.0 and FES 95.2. Mapping RMS residuals of the tidally corrected SSH facilitates comparisons among models under the assumption that the one yielding the lowest RMS is the ''best'' in the least squares sense. It also allows areas of significant tidal errors to be identified where mesoscale variability is known to be modest (e.g., Noumea), as in our interpretation. However,

where mesoscale eddies or boundary current meanders are dominant (as in the Tasman Sea) these will inflate the RMS. Fitting a pure sinusoid with a period corresponding to that of the tidal constituent alias allows error levels to be identified for specific spectral lines. It thus better discriminates potential alias errors from the low frequency background than does the RMS method. Although it also removes quasi-oscillatory low frequency variability present in the same wave band, this effect will diminish for longer records, which allow finer resolution of the spectral line, thus reducing noise. In practice we used this method only for the major constituent, M2, which is the dominant error source, but genuine low frequency signals in the 60 day wave band might also have been removed.

[50] Optimally lagged correlation analysis of the low frequency SSH residuals and GCAs, with similarly filtered in situ data, is clearly not a direct test for tidal errors per se. However, altimetry data retaining significant tidal errors is unlikely to correlate well with low frequency in situ data, as found for CSR 3.0 near Mackay; so tidal error could explain a low correlation where other evidence suggests it should be high. The method also gives information on the direction and speed of propagation (phase velocity) of disturbing influences. However, its application in this context should be regarded as experimental. The results are subject to statistical uncertainties such as phase ambiguities associated with oscillatory signals. Interpretation also requires a careful distinction between particle velocities (current velocities) and speed and direction of wave or eddy propagation (phase velocities), which will differ, depending on the dynamics. Finally all these techniques may be subject to aliasing errors. We have sought to minimize spatial aliases by sampling SSH along tracks, but aliasing associated with large track to station separations could cause spurious correlations. Temporal aliasing of weather band signals by the 10 day TOPEX repeat cycle could influence such analyses.

[51] RMS SSH plots show generally lower levels in the Coral Sea than in the Tasman Sea, where mesoscale eddies and the meandering Tasman front are energetic sources of variability. To the north it rises to a broad maximum close to the path of the inflowing SEC [*Andrews and Clegg*, 1989; *Burrage et al.*, 1995]. With the exception of areas affected by local topography and tidal errors, the RMS variability in the Coral Sea was consistent with what is known of the general circulation. For example, there was a local maximum near the location of the Papuan Gyre [*Burrage*, 1993]. The high RMS variability off Mackay, which in some previous studies has appeared as evidence of high mesoscale variability [e.g., *Shum et al.*, 1997, Plate 4] is effectively eliminated when the SGBR regional tidal model is employed (Figure 6). The high RMS surrounding the Solomon Islands is unlikely to be due to tidal errors, but may result from seasonal circulation around the islands and/or data dropouts. The high RMS north and east of the Solomons, however, is mostly likely caused by genuine mesoscale variability associated with the northern limb of the South Pacific subtropical gyre.

[52] The M2 alias amplitude plots generally clarify and support our interpretation of the RMS variability. They confirm the presence of substantial tidal errors near Broad Sound/Mackay and over the broad continental shelf in the Gulf of Papua. The slightly elevated tidal error levels in the western Tasman Sea, however, may be a result of genuine mesoscale energy present in the 60-day wave band. They also confirm the low tidal alias errors near the Solomon Islands.

[53] Several authors have reported applications of regional tidal models to correct altimetry in coastal areas. *Ray* [1999] presents a newly developed global ocean model, GOT99.2, based on the earlier *Schrama and Ray* [1994] model, but assimilating 3 times the amount of TOPEX altimeter data. Using a regional a priori hydrodynamic model in the Gulf of Maine, he found a significant reduction in RMS residuals to levels of order 10 cm, in comparison with CSR 4.0. *Kantha et al.* [1994] applied regional models forced by global tidal models offshore and produced operationally useful analyses of TOPEX altimetry in coastal areas. Our application of the SGBR regional tidal model showed that effective tidal corrections can be deduced in areas affected by the presence of reefs and islands, provided care is taken to account for the influence of subgridscale topography.

[54] Numerous studies have compared tidally corrected SSH data with tide gauge records [e.g., *Mitchum*, 1994; *Nerem et al.*,1994; *Le Provost*, 1994; *Koblinsky*, 1999]. Actual calibration studies [*Born et al.*, 1994; *Christensen et al.*, 1994; *Ménard et al.*, 1994; *White et al.*, 1996; *Exertier et al.*, 2000] seek to compare absolute levels from TOPEX at, or carefully extrapolated to, the calibration site, and have demonstrated RMS differences ranging from to about 1.5 to 3.5 cm. Studies using non-coincident coastal and island tide gauges, pressure gauges or inverted echosounders, and dynamic heights computed from temperature sensors [*Katz et al.*, 1995; *Mitchum*, 1994; *Picaut et al.*, 1995; *Verstraete and Park*, 1995; *Woodworth et al.*, 1996; *Murphy et al.*, 1996] generally achieve RMS differences ranging between about 4 and 12 cm, depending upon location, with correlations ranging from 0.4 to 0.9, but typically 0.6 to 0.7. The results we report here are consistent with these ranges, but may be less conservative (larger than would otherwise be the case) because we have optimized lags and locations to account for phase propagation. Our results could also be more variable as they are obtained from individual locations, not global averages.

[55] Some investigators [e.g., *Mitchum*, 1994] correlate SSH data from the track point of "closest approach" to the in situ station. Others [e.g., *Koblinsky et al.*, 1999] have examined the correlation at various places along track, as has been done here. *Mitchum* [1994] found a significant but weak dependence of correlation upon track-to-station separation for tracks adjacent to stations, considering only the point of closest approach. Our results, and those of *Koblinksky* [1999], show that correlation usually falls off more or less symmetrically along track, either side of the optimum lag location. However, in some cases we found evidence of spatial or temporal double maxima. This effect could be explained by anomalies being diverted and/or split around an island or reef site away from the point of closest approach. We also plotted the optimum lag correlation as a function of distance from station (Figure 14). The results for monthly smoothed data (Figure 14a) show that, if Honiara is omitted, there is tendency for the envelope of the optimal correlation values to decrease with increasing separation.

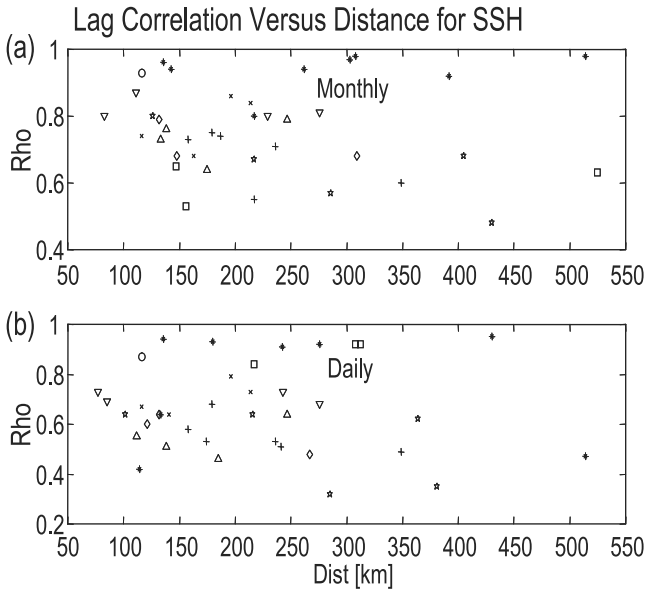

Figure 14. Optimal lag correlation for (a) monthly and (b) daily smoothed sea levels as a function of distance between in situ station and optimum correlation point along the adjoining track. Markers refer to stations FF (circle), PV (cross), LT (plus), HA (asterisk), BB (square), CF (diamond), OR (triangle down), FR (triangle up), RB (star).

This is less evident for the daily data (Figure 14b) and few of the individual stations show any consistent trend. Clearly topographic complexities and regional circulation dominate distance in determining the correlation.

[56] *Mitchum* [1994] experimented with applying lag adjustments for westward drift at the first mode baroclinic Rossby wave speed [*Gill*, 1982, p. 489], and discussed possible departures due to non-Rossby wave dynamics and other factors. Meridional as well as zonal drift needs to be taken into account where topographic features govern eddies or boundary currents, and Rossby wave dynamics may not apply.

[57] We experimented with his approach by computing zonal and meridional phase propagation velocities from optimal lags and scaling them by the local Rossby phase speed. None of the phase velocities showed evidence of sea level anomalies drifting west at the Rossby speed. Instead, there was evidence of predominantly eastward and southward propagation off the NE Australian shelf, consistent with the general motion of the EAC. Phase propagation was eastward at Port Vila and north-eastward at Funafuti. The latter results are not easily explained. They contrast with those of *Vivier et al.* [1999], which assign a dominant role to (mostly annual period) westward Rossby wave propagation in the western South Pacific, including the Coral Sea. Their results are based on a TOPEX data assimilation procedure which models the waves kinematically in an attempt to eliminate local influences. Our results, however, might be significantly influenced by station locations, which are arrayed around the Coral Sea margins, rather than in the interior, and by other site specific factors. This needs further investigation and might be resolved by track to track cross-correlation of the SSH data in the region, independently of the in situ data.

[58] The phase lags at certain localities appear to reflect delays in the response of the in situ station to the surrounding deep ocean, possibly due to local topographic influences with attendant amplification or attenuation of SSH signals. We should not read too much into individual lag and regression coefficient values, however, as these are subject to statistical uncertainties. Lags and correlations might also be frequency dependent. In this case, coherence rather than correlation analysis would be more appropriate, and is recommended for future studies when longer and more complete data sets are available. Alternatively, the data could be band-pass filtered and correlated within different wave bands. Finally, removal of the strong seasonal signal from both data sets prior to correlation could be tried to reduce the possibility of spurious correlations related to localised seasonal variability (e.g., seasonal heating inside a reef lagoon or wind-induced coastal upwelling), but at the risk of removing a dominant signal of interest.

[59] Purpose-built sea level verification sites and reference stations with a predictable relationship to the TOPEX tracks have been effectively used to validate altimetry and monitor altimeter drift over time [e.g., *Mitchum*, 1994]. However, comparison of altimetric SSH and in situ sea levels for shallow or non-coincident locations on a regional scale might best be viewed as an opportunity to investigate the characteristics and representativeness of each site, rather than as validation per se. Comparisons with such stations will likely produce conservative error estimates in contrast to sites that are ideally located on TOPEX ground tracks. *Kagan and Kivman* [1994] present a necessary condition of representativeness of sites located at islands and in island archipelagos for deep ocean tides, which could possibly be extended to lower frequency motions to help assess such effects.

[60] The SSHs were also compared with long-term records from pressure gauges maintained at off-shelf reefs by AIMS since 1988. Datum shifts were adjusted by ascribing the corresponding TOPEX mean sea level to each data segment. While this artificially improved the correlation, it enabled us to demonstrate that shorter-term (intraseasonal) fluctuations are also well correlated. Hence relatively economical pressure gauges can provide the higher frequency fluctuations that are aliased by the 10 day repeat cycle, while the altimetry provides the long-term trends.

[61] Finally, GCAs were computed from the Topex SSH data and compared with de-meaned low frequency along slope currents using optimal lagged correlation analysis. The results showed modest to high correlation (order 0.5 and 0.8, respectively off Jewell and Myrmidon Reefs, respectively) and sensible phase propagation directions. The relationship between the two time series appears stable, with no obvious year-to-year biases in the current meter records over the 3.6 year period. Thus means deduced from other methods, once known, should remain stationary (statistically), so that absolute currents as well as seasonal and interannual variability could be reliably inferred. The poorer correlation between GCAs and currents at Jewell Reef may be due to the close proximity to the reef and attendant tidal errors, the relatively large track to station separation, along with possible flow separation and migration over time of the near-surface SEC bifurcation past the mooring location.

[62] Correlation of the TOPEX ground tracks that intersect the GBR was hampered by the lack of adequate tidal corrections close to the shelfbreak and within the GBR lagoon, except in the southern GBR, where the high-resolution regional tidal model was applied. The model domain has recently been expanded to include the central and northern GBR continental shelf and slope and thus facilitate extraction of SSH along additional altimeter ground tracks. Further work is needed to isolate the effects of dropouts over reefs and islands, and to vary data screening criteria in order to optimize data returns near such features. The TMR wet troposphere correction must also be extrapolated horizontally if TOPEX data are to be utilized close to the coast. Since the radiometer has a 40 km footprint diameter (half power beam width, *Janssen et al.* [1995]), its brightness temperatures may be contaminated by land within a radial distance of about 20 km.

6. Conclusions

[63] The performance of the standard CSR3.0 global tidal model corrections in the Coral Sea was assessed using collinear track analysis and found to be generally adequate in the Coral Sea, away from the larger reefs and islands. However, it is deficient off the NE Australian continental shelf/Great Barrier Reef, particularly in the macro-tidal area near Broad Sound and Mackay. To provide tidal corrections in this area we employed a high-resolution numerical hydrodynamic tidal model of the region.

[64] A novel application of optimal lagged correlation techniques to the tidally corrected low frequency SSH shows very high correlation (>0.9) for Honiara, owing to the M2 amphidrome. It remains satisfactorily high (>0.6) for locations in both the eastern and western Coral Sea, and in the Southern GBR within the regional tidal model domain. Inferred phase propagation velocities near the in situ stations vary widely, apparently in response to the competing influences of local topography, regional circulation features and timescales. Time series of Geostrophic Current Anomalies from in situ current meter moorings on the continental slope give optimal lagged correlations of order 0.5, and 0.8 near Jewell (14 S) and Myrmidon Reef (19 S), respectively.

[65] Our study region included the topographically complex Coral Sea and adjoining NE Australian continental slope, and the southern entrance to the GBR Lagoon, where tides are amplified as they propagate around the reef matrix and over an expansive continental shelf. We conclude that, when coupled with accurate tidal models of sufficient resolution, TOPEX altimetry can provide useful information on long-term sea levels and geostrophic currents in regions subject to strong topographical constraints and macro-tidal influences.

Appendix A: Data Acquisition and Analysis

A.1. In Situ Tide Gauges

[66] To supplement data from established TOPEX reference stations (*Shum et al.* [1997, Figure 4] shows representative locations; a gap in the western Coral Sea being evident), we obtained high accuracy and precision data from the SEAFRAME tide gauge network. This network is operated by the Australian National Tidal Facility (NTF) (http://www.ntf.flinders.edu.au). SF stations in our area of interest include: Cape Ferguson, Rosslyn Bay, Honiara, Port Vila, Lautoka and Funafuti (Table 1, Figure 2). The primary, AQUATRAK, sensor used in the SF gauges has a sample resolution of 1 mm. Datum changes monitored so far by the Australian Surveying and Land Information Group (http://www.auslig.gov.au) are generally less than 1 mm yr^{-1} and thus negligible compared with expected tidal errors. The 6 min sampled sea level data are filtered and decimated to hourly intervals, while weather and ancillary data are recorded hourly. Sea level and atmospheric pressure data files, edited and archived by NTF were processed at the Australian Institute of Marine Science (AIMS) using in-house MATLAB (The Mathworks Inc.) software. Records used ran from 1992 to 1996, where available, to span the first 132 cycles or 3.61 yr of TOPEX altimetry data. Harmonic analyses were performed on the hourly in situ time series data (see appendix B.1), while for comparison with tidally corrected TOPEX data, the tides were removed using a low-pass filter. The filters used were 51 hour (2.1 day) or 1440 hour (60 day) long raised cosine (Hamming) filters, which have cut-off periods (first zero points) of 25.5 hr and 30 day. Both retain the longer timescales, but the latter also removes weather band variability and reduces noise levels. For convenience we refer to these time series as being smoothed on ''daily'' or ''monthly'' timescales, respectively.

[67] Data from other Pacific Island sites were obtained from the University of Hawaii Sea level Center (UHSLC). The format and our processing were similar to that described for the NTF data. These tide gauges are in most cases conventional stilling well instruments, which are less precise and accurate than the SF acoustic tide gauge stations. The main conventional tide gauge sites used in our comparisons were Townsville, Bundaberg, Noumea and Funafuti (Table 1, Figure 2).

[68] Long-term sea level data have also been obtained by AIMS using repeated subsurface pressure gauge deployments of Aanderaa WLR5 and WLR7 Water Level Recorders, located both at shelf edge and off-shelf reef sites (see B&S for deployment details). Commencing late in 1987, these deployments, are part of a long-term AIMS program to examine Transports of the East Australian Current System (TEACS). Only results from the Carter Reef, Osprey Reef, Flinders and Myrmidon Reef TEACS pressure gauges (Table 1, Figure 2) are employed here. For convenience we group the pressure gauges with the conventional tide gauges described above and henceforth use the capitalised term ''Tide Gauges'' or TG to refer to the two collectively and in distinction from the SF acoustic gauges. The lower case ''tide gauges'' refers generically to all three types.

[69] In contrast to the conventional tide gauges which are attached to permanent man-made structures, the TEACS pressure gauges are deployed by divers on partially buried and/or staked concrete disks set onto a sandy seabed or coral reef flat. The disk allows 2 instruments to run in tandem during changeovers to intercalibrate them and maintain the datum, but otherwise we rely upon manufacturer calibrations. Used alone, the data are best suited to the

study of higher frequency (seasonal through weather-band to tidal) time-scales. However, the long record (up to 10 years) provides many degrees of freedom and facilitates reliable statistical estimates of processes operating at these shorter timescales. Interannual and longer-term sea level changes cannot be reliably observed due to datum uncertainties, but we have found we can use long term means of the TOPEX altimetry to detect and correct for undocumented datum changes.

[70] We used a variety of procedures and checks to preserve datum continuity and verify the quality of the pressure gauge data. We cross-calibrated instruments in the field where possible to maintain a fixed, but arbitrary, datum for multiyear periods. We looked for possible changes in calibration as specific instruments were redeployed at different array locations. Other checks included screening for instrumental, sampling and recording errors, and detecting timing or datum changes in the instrumental response to the tides. Short data gaps (less than 1 day) or instrument displacements were corrected by matching tidal predictions preceding and following the record discontinuity. This method assumes low frequency variations are minimal during the break. For longer gaps we adjusted the mean sea level of the pressure gauge data segment to match that computed from the TOPEX altimetry data. This method was applied to Osprey and Flinders Reef time series where there was no other possibility of recovering the datum. Naturally, this precludes any independent check on long-term TOPEX-derived sea level trends at these stations.

[71] After applying these checks and corrections, the 6 years or longer TG records from the Osprey and Flinders Reef off-shelf sites and the Myrmidon Reef outer-shelf site were deemed suitable for extracting semi-diurnal through monthly tidal constituents (e.g., Figure 3a, Osprey Reef not shown). In addition, the FR and MR data are suitable for analysing long-term trends for periods up to about 6 years, but with some caveats due to possible instrumental calibration changes and long-term drift. With datum adjustment using TOPEX, Osprey Reef can also be used for this purpose. Since most of the SF stations have by now yielded data sets of similar duration, they have also been harmonically analysed (Figure 3b).

[72] For comparison with the SSH data, which is adjusted using the inverse barometer correction provided in the Geophysical Data Record, the conventional tide gauge data were similarly adjusted for atmospheric pressure variations. This was done conventionally by multiplying the coincident atmospheric pressure departure from the standard atmosphere of 1013.25 HPa by a factor 0.0099908 $m(Hpa)^{-1}$ and adding this product to the sea level. This adjustment is not made to the TEACS pressure gauges, as these directly measure total (sea level plus atmospherically induced) pressure, which is the required dynamical quantity.

A.2. Current Meters

[73] Data were also obtained from two long-term TEACS current meter moorings located on the upper continental slope seaward of Jewell (14 S) and Myrmidon Reefs (19 S) in water depths of 352 and 200 m, respectively (Table 1, Figure 1). These moorings, which are fitted with Aanderaa RCM7 current meters at depths of 32 m and 70 m (JW1–2), and at 25, 50, 75 and 150 m (MY1–4), have been maintained since October 1986 and August 1987, respectively (see B&S for long-term mooring deployment and data analysis details). The long-term current meter data were processed using analogous methods and the same filters as those used for the sea level data.

Appendix B: Data Analysis

B.1. Tide Gauge Data Harmonic Analysis

[74] Tidal analyses were performed using least squares harmonic analysis software written by the third author (LBM) and based on the techniques of *Foreman* [1977]. The software employs the same principles, but makes the necessary nodal adjustments automatically at appropriate time intervals. The variables A_{jk}, the "Element of Interaction," which Foreman assumes is 1.0 for records as long as 1 year, are calculated explicitly. This is important as we are analysing long records where A_{jk} will, at times, be close to zero.

[75] To test the software, long-term sea level data from the TOPEX "reference station" at Funafuti obtained from the UHSLC were re-analysed and the results compared with published analyses. Our analysis agreed to within ~1mm in amplitude with the reference analysis which was restricted to a single year (1985), thus demonstrating reliability of our analytical methods. However, the multi (9) year-analysis uncovered an anomaly in the M2 constituent at Funafuti. Multiple single year analyses produced an unstable result with the M2 amplitude varying by about 10%. This result calls into question the representativeness of the reference M2 analysis for this Station, ST103 (#92 [see *Le Provost*, 1994]).

[76] After software validation, long-term harmonic analyses were performed on the data from the various TG and SF sites. For the TG stations, over 9.8 years of data were analysed from each of Townsville, Noumea and Funafuti and over 5.5 years at Myrmidon and Flinders Reefs. Records from the SF sites which typically begin in 1992 were analysed over the 4 year period spanning the TOPEX MGA data set (appendix B.2). Analyses from the Townsville tide gauge and the nearby Cape Ferguson SF were similar (Figures 3a and 3b), which gives us confidence that the two different station types are comparable.

[77] At the suggestion of an anonymous reviewer, we investigated seasonal variation in the tidal constants which could be ascribed to contributions from the internal tide (particularly M2) to observed sea level variations. We analysed tide gauge data from FR, OR, MR and CR then computed tidal band residuals. While FR and OR are at off-shelf reefs, MR is on the upper slope and CR on the outer shelf. Although we found no evidence of significant seasonality in the residuals, there was some evidence of a spring-neap cycle. This suggests there is some tidal energy, presumably baroclinic that is neither resolved by the analysis nor phase-locked to the barotropic tide, nor seasonal in character. The RMS tidal residuals were 2.3 cm at FL and CR and 2.6 cm at OR and MR. This represents a rather small "noise" contribution of 3.4% at MR when the RMS residual of 2.6 cm is compared with an RMS M2

value of 76.4 cm (corresponding to amplitude 54 cm, Figure 3a).

B.2. TOPEX Altimetry

[78] The TOPEX/Poseidon altimeter data up to cycle 132 were obtained from the Geophysical Data Records (GDRs) available on the PO.DAAC Merged GDR Version A CD ROMs. Data were processed using a suite of FORTRAN programs originally developed for GEOSAT that were adapted for our purpose. Processing followed these two steps:

[79] 1. The original pass files were read and edited using a range of criteria designed to eliminate altimetric and environmental correction data which were incomplete, erroneous or spanned arcs of insufficient length [*Benada*, 1993]. All standard environmental corrections were made, but tidal corrections were deferred, and orbit error adjustments and geoid corrections were omitted. On the basis of orbit adjustment experiments [R. Coleman, personal communication, 1994; *Naeije*, 1995] it is not only unnecessary to remove orbit errors for routine oceanographic applications, but difficult to do so, without compromising oceanographic information. The pass data were interpolated to a 0.05 deg latitude grid to simplify processing, and sequenced as a time series of sea surface height deviations for each grid point along each ground track. The interpolation was done using a 6 km long Gaussian filter.

[80] 2. The resulting much smaller ''pass'' files were corrected using one of the optional global or regional tidal models. At each grid point of a given track, statistics including mean and RMS altimetric heights were saved for future use along with the primary data set, i.e., an array of SSH deviations relative to the temporal mean over all cycles processed for each grid point, indexed by latitude grid point and cycle number. After some experimentation the altimeter drift correction was omitted, since its effect over the 3.6 year period is small compared with tide gauge error and we are not attempting to resolve long-term trends. We also trialed, but finally excluded, the short interleaved Poseidon altimeter data segments, thus avoiding the effects of range offsets between the two instruments.

[81] To reduce noise levels for statistical analysis, the along-track smoothed (6 km cutoff) altimetry data were further filtered in the along-track direction using a 32 km (SGBR model domain) or 72 km (CSR 3.0 domain) box car low-pass filter. The characteristically shorter box car filter was selected over other filters, in spite of its relatively poor side lobe behaviour, to minimize filter loss near coasts and islands. Filter lengths were chosen, after experimentation, to reduce noise levels while resolving topographically induced spatial variations.

[82] The altimetry data were also low-passed using a 6 cycle (60 day) long Hamming filter (Tc = 30 day) for comparison with the monthly smoothed in situ data, so that both filters were 60 day long (Tc = 30 day). No smoothing in time was necessary for the tidally corrected SSH data used for comparison with the daily smoothed in situ data.

Appendix C: TOPEX Tidal Models

[83] The standard tidal models available on the POMGA version of the TOPEX PO.DAAC merged GDRs (Cycles 1 to 132) are the modified enhanced *Schwiderski* [1980] model [*Le Provost et al.*, 1991] and the *Cartwright and Ray* [1990] model derived from GEOSAT altimetry. Both these models are independent of the TOPEX data, although the latter is derived from an alternative altimetric source. The newer POMGB version includes the hybrid models CSR 3.0 [*Eanes and Bettadpur*, 1995] and FES95.2 [*Le Provost et al.*, 1998] models. These utilize both hydrodynamic model results and altimetry data to construct a global tidal solution.

[84] We used the POMGA version GDRs, but obtained the newer (CSR3.0 and FES95.2) tidal model data and prediction software available from ftp sites. The range of constituents provided varies. Most models have options for computing the elastic ocean tide (ocean plus load tide, see *Benada* [1993] for definitions), which is needed when correcting TOPEX altimetry for comparisons with sea level records from Earth-fixed stations. The hybrid models (CSR 3.0, FES 95.2) provide appropriate load tide corrections which we included in the total tide prediction along with equilibrium tidal solutions for the minor constituents.

[85] **Acknowledgments.** The National Tidal Facility at Flinders University and the University of Hawaii Sea Level Centre supplied sea level data, and surface pressure data were obtained from the Australian Bureau of Meteorology. The authors acknowledge funding and infrastructure support from the Australian Institute of Marine Science, and from the School of Mathematical and Physical Science and the CRC Reef Research Centre, Ltd., James Cook University. DB wishes to thank S. Massel formerly of AIMS and D. Williams and P. Doherty (AIMS) for their patience and encouragement throughout the study. TOPEX altimeter data was provided through the joint efforts of NASA/CNES data centres through the authors' membership of the TOPEX Science Working Team. M. Schlax and D. Chelton (Oregon State University), and Neil White (CSIRO) provided early versions of altimetry processing code that were adapted for our work.

References

Amin, M., and G. W. Lennon, On anomalous tides in Australian waters, *Int. Hydrogr. Rev.*, *1*, 151–168, 1992.

Andrews, J. C., and L. Bode, The tides of the central Great Barrier Reef, *Cont. Shelf. Res.*, *8*, 1057–1085, 1988.

Andrews, J. C., and S. Clegg, Coral Sea circulation and transport deduced from modal information models, *Deep Sea Res.*, *36*, 6957–6974, 1989.

Ayoub, N., P.-Y. Le Traon, and P. De Mey, A description of the Mediterranean surface variable circulation from combined ERS-1 and TOPEX/POSEIDON altimetric data, *J. Mar. Syst.*, *18*, 3–40, 1998.

Benada, R., Merged GDR (TOPEX/Poseidon) Users Handbook, Version 1.0, -11007, JPL Phys. Oceanogr. (PODAAC) DAAC, Pasadena, Calif., 1993.

Bendat, J. S., and A. G. Piersol, *Random Data Analysis and Measurement Procedures*, 566 pp., John Wiley, New York, 1986.

Bode, L., The Reef, tides, and Flinder's perspicacity, *Oceanus*, *29*, 86–87, 1986.

Bode, L., and L. B. Mason, Tidal modelling in Torres Strait and the Gulf of Papua, in *Recent Advances in Marine Science and Technology*, edited by O. Bellwood, H. Choat, and N. Saxena, pp. 55–65, PACON Int., Honolulu, Hawaii, 1995.

Bode, L., L. B. Mason, and J. H. Middleton, Reef parameterisation schemes with application to tidal modelling, *Prog. Oceanogr.*, *40*, 285–324, 1997.

Bonnefond, P., P. Exertier, P. Schaeffer, S. Bruinsma, and F. Barlier, Satellite altimetry from a short-arc orbit technique: Application to the Mediterranean, *J. Geophy. Res.*, *100*, 25,365–25,382, 1995.

Born, G. H., M. E. Parke, P. Axelrad, K. L. Gold, J. Johnson, K. W. Key, and D. G. Kubitschek, Calibration of the TOPEX altimeter using a GPS Buoy, *J. Geophys. Res.*, *99*, 24,517–24,626, 1994.

Burrage, D. M., Coral Sea currents, The seas around us - Number 3, *Corella*, *17*, 135–145, 1993.

Burrage, D. M., J. A. Church, and C. R. Steinberg, Linear systems analysis of momentum on the continental shelf and slope of the Central Great Barrier Reef, *J. Geophys. Res.*, *96*, 22,169–22,190, 1991.

Burrage, D. M., K. P. Black, and K. F. Ness, Long-term current prediction on the continental shelf of the central Great Barrier Reef, *Cont. Shelf. Res.*, *14*, 803–829, 1994.

Burrage, D. M., R. D. Hughes, L. Bode, and D. B. McWilliams, Dynamic features and transports of the Coral Sea circulation, in *Recent Advances in Marine Science and Technology*, edited by O. Bellwood, H. Choat, and N. Saxena, pp. 95–105, PACON Int., Honolulu, Hawaii, 1995.

Burrage, D. M., C. R. Steinberg, W. J. Skirving, and J. A. Kleypas, Mesoscale circulation features of the Great Barrier Reef Region inferred from NOAA Satellite Imagery, *Remote Sens. Environ.*, *56*, 21–41, 1996.

Burrage, D., L. Bode, C. Steinberg, and L. Mason, North Australian Tropical Seas Circulation Study (Phase IV) TOPEX/Poseidon: 5 years of progress, *AVISO Altimetry Newsl.*, *6*, 18–20, 1998.

Cartwright, D. E., and R. D. Ray, Oceanic tides from Geosat altimetry, *J. Geophys. Res.*, *95*, 3069–3090, 1990.

Cartwright, D. E., and R. D. Ray, Energetics of global ocean tides from Geosat altimetry, *J. Geophys. Res.*, *96*, 16,897–16,912, 1991.

Church, J. A., J. C. Andrews, and F. M. Boland, Tidal currents in the central Great Barrier Reef, *Cont. Shelf Res.*, *4*, 515–531, 1985.

Christensen, E. J., et al., Calibration of TOPEX/POSEIDON at Platform Harvest, *J. Geophys. Res.*, *99*, 24,465–24,485, 1994.

Desai, S. D., and J. M. Wahr, Another ocean tide model derived from TOPEX/POSEIDON satellite altimetry, *Eos Trans. AGU*, *75*(44), Fall Meet. Suppl., F57, 1994.

Eanes, R. J., and S. V. Bettadpur, The CSR3.0 global ocean tide model, *CSR-TM-95-06*, Cent. for Space Res., Univ. of Tex. at Austin, 1995.

Egbert, G. D., A. F. Bennett, and M. G. G. Foreman, TOPEX/POSEIDON tides estimated using a global inverse model, *J. Geophys. Res.*, *99*, 24,821–24,852, 1994.

Exertier, P., P. Bonnefond, O. Laurain, F. Barlier, Y. Menard, E. Jeansou, A. Orsoni, B. Haines, D. Kubitschek, and G. Born, Absolute altimeter calibration in Corsica, *AVISO Alimetry Newsl.*, *7*, 28–31, 2000.

Foreman, M. G. G., *Manual for Tidal Heights Analysis and Prediction*, 101 pp., *Pacific Mar. Sci. Rep. 77-10*, Inst. of Ocean Sci., Patricia Bay, B. C., 1977.

Foreman, M. G. G., W. R. Crawford, J. Y. Cherniawsky, J. F. R. Gower, L. Cuypers, and V. A. Ballantyne, Tidal correction of TOPEX/POSEIDON altimetry for seasonal sea surface elevation and current determination off the Pacific coast of Canada, *J. Geophys. Res.*, *103*, 27,979–27,998, 1998.

Gill, A. E., *Atmosphere-Ocean Dynamics*, 662 pp., Academic, San Diego, Calif., 1982.

Griffin, D. A., J. H. Middleton, and L. Bode, The tidal and longer-period circulation of Capricornia, southern Great Barrier Reef, *Aust. J. Mar. Freshwater Res.*, *38*, 461–474, 1987.

Hughes, R. D., An investigation of the Coral Sea with an ocean general circulation model, Ph.D. thesis, James Cook Univ., Townsville, Australia, 1993.

Janssen, M. A., C. S. Ruf, and Stephen J. Keihm, TOPEX/Poseidon Microwave Radiometer (TMR): II. Antenna pattern correction and brightness temperature algorithm, *IEEE Trans. Geosci. Remote Sens.*, *33*, 1138–1146, 1995.

Kagan, B. A., and G. A. Kivman, A necessary condition for the representativeness of island tidal measurements, *J. Geophys. Res.*, *100*, 11,047–11,051, 1994.

Kantha, L. H., P. E. Pontius, and D. M. Beitzell, Tides and altimetry in marginal and semi-enclosed seas, *Eos Trans. AGU*, *75*(44), Fall Meet. Suppl., F57, 1994.

Katz, E. J., A. Busalacchi, M. Bushnell, F. Gonzalez, L. Gourdreau, M. McPhaden, and J. Picaut, A comparison of coincidental time series of the ocean surface height by satellite altimeter, mooring and inverted echo sounder, *J. Geophys. Res.*, *100*, 25,101–25,108, 1995.

Koblinsky, C. J., R. D. Ray, B. D. Beckley, A. Brenner, L. S. Tsaoussi, and Y.-M. Wang, *NASA Ocean Altimeter Pathfinder Project Report 2: Data Set Validation,NASA/TM-1999-209230*, NASA, Goddard Space Flight Cent., Greenbelt, Md., 1999.

Larnicol, G., P.-Y. Le Traon, N. Ayoub, and P. De Mey, Mean sea level and surface circulation variability of the Mediterranean Sea from 2 years of TOPEX/POSEIDON altimetry, *J. Geophys. Res.*, *100*, 25,163–25,177, 1995.

Le Provost, C., A new in situ reference data set for ocean tides, *AVISO Altimetry Newsl*, *3*, 1994.

Le Provost, C., F. Lyard, and J. M. Molines, Improving ocean tide prediction by using additional semi-diurnal constituents from spline interpolation in the frequency domain, *Geophys. Res. Lett.*, *18*, 845–848, 1991.

Le Provost, C., M. L. Genco, F. Lyard, P. Vincent, and P. Canceil, Spectroscopy of the world ocean tides from a finite element hydrodynamic model, *J. Geophys. Res.*, *99*, 24,777–24,797, 1994.

Le Provost, C., F. Lyard, J. M. Molines, M. L. Genco, and F. Rabilloud, A hydrodynamic ocean tide model improved by assimilating a satellite altimeter-derived data set, *J. Geophys. Res.*, *103*, 5513–5529, 1998.

Ma, X. C., C. K. Shum, R. J. Eanes, and B. D. Tapley, Determination of ocean tides from the first year of TOPEX/POSEIDON altimeter measurements, *J. Geophys. Res.*, *99*, 24,809–24,820, 1994.

Ménard, Y., (Ed), *Minutes of the Second Joint TOPEX/POSEIDON and Jason-1 ScienceWorking Team Meeting*, *Ref TP2-J0-CR-1425-CNES*, Centre National d'Etudes Spatiales, Toluouse, France, 1999.

Ménard, Y., E. Jeansou, and P. Vincent, Calibration of the TOPEX/POSEIDON altimeters at Lampedusa: Additional results at Harvest, *J. Geophys. Res.*, *99*, 24,487–24,504, 1994.

Middleton, J. H., V. T. Buchwald, and J. M. Huthnance, The anomalous tides near Broad Sound, *Cont. Shelf Res.*, *3*, 359–381, 1984.

Mitchum, G. T., Comparison of TOPEX sea surface heights and tide gauge sea levels, *J. Geophys. Res.*, *99*, 24,541–24,553, 1994.

Molines, J. M., C. Le Provost, F. Lyard, R. D. Ray, C. K. Shum, and R. J. Eanes, Tidal corrections in TOPEX/POSEIDON Geophysical Data Records, *J. Geophys. Res.*, *99*, 24,749–24,760, 1994.

Murphy, C. M., P. Moore, and P. Woodworth, Short-arc calibration of the TOPEX/POSEIDON altimeters at Lampedusa: Additional results at Harvest, *J. Geophys. Res.*, *101*, 14,191–14,200, 1996.

Naeije, M. C., Evaluating 2 Years' Worth of TOPEX/POSEIDON Sea Level Data, *TOPEX/POSEIDON Res. News*, *410-42*(4), 17–22, 1995.

Nerem, R. S., E. J. Schrama, C. J. Koblinsky, and B. D. Beckley, A preliminary evaluation of ocean topography from the TOPEX/POSEIDON mission, *J. Geophys. Res.*, *99*, 24,565–24,583, 1994.

Parke, M. E., R. H. Stewart, D. L. Farless, and D. E. Cartwright, On the choice of orbits for an altimetric satellite to study ocean circulation and tides, *J. Geophys. Res.*, *92*, 11,693–11,707, 1987.

Picaut, J., A. J. Busalacchi, M. J. McPhaden, L. Gourdeau, F. I. Gonzalez, and E. C. Harckert, Open-ocean validation of TOPEX/POSEIDON sea level in the western equatorial Pacific, *J. Geophys. Res.*, *100*, 25,109–25,127, 1995.

Ray, R. D., *A Global Ocean Tide Model from TOPEX/POSEIDON Altimetry: GOT99. 2*, NASA, Goddard Space Flight Cent., Greenbelt, Md., 1999.

Schrama, E. J. O., and R. D. Ray, A preliminary tidal analysis of TOPEX/POSEIDON Altimetry, *J. Geophys. Res.*, *99*, 24,799–24,808, 1994.

Schwiderski, E. W., On charting global ocean tides, *Rev. Geophys.*, *18*, 243–268, 1980.

Shum, C. K., et al., Accuracy assessment of recent ocean tide models, *J. Geophys. Res.*, *102*, 25,173–25,194, 1997.

Verstraete, J.-M., and Y.-H. Park, Comparison of TOPEX/POSEIDON altimetry and in situ sea level data at Sao Tome Island, Gulf of Guinea, *J. Geophys. Res.*, *100*, 25,129–25,134, 1995.

Vivier, F., K. A. Kelly, and L. A. Thompson, Contributions of wind forcing, waves, and surface heating to sea surface height observations in the Pacific Ocean, *J. Geophys. Res.*, *104*, 20,767–20,788, 1999.

Webb, D. J., On the age of the semi-diurnal tide, *Deep Sea Res.*, *20*, 847–852, 1973a.

Webb, D. J., Tidal resonance in the Coral Sea, *Nature*, *243*, 511, 1973b.

White, N. J., R. Coleman, J. A. Church, P. J. Morgan, and S. J. Walker, A southern hemisphere verification for the TOPEX/POSEIDON satellite altimeter mission, *J. Geophys. Res.*, *101*, 11,935–11,947, 1996.

Wolanski, E., *Physical Oceanographic Processes of the Great Barrier Reef*, CRC Press, Boca Raton, Fla., 1994.

Wolanski, E., and G. L. Pickard, Long-term observations of currents on the central Great Barrier Reef continental shelf, *Coral Reefs*, *4*, 47–57, 1985.

Woodworth, P. L., J. M. Vassie, C. W. Hughes, and M. P. Meredith, A test of the ability of TOPEX/POSEIDON to monitor flows through Drake Passage, *J. Geophys. Res.*, *101*, 11,935–11,947, 1996.

L. Bode, School of Mathematical and Physical Sciences, James Cook University, Queensland, 4811, Australia. (lance.bode@jcu.edu.au)

D. Burrage, Department of Marine Science, University of Southern Mississippi, Box 1020, Stennis Space Center, MS 39529, USA. (burrage@usm.edu)

L. B. Mason, School of Engineering, James Cook University, Queensland, 4811, Australia. (luciano.mason@jcu.edu.au)

C. Steinberg, Australian Institute of Marine Science, PMB No 3, Townsville, Queensland, 4810, Australia. (c.steinberg@aims.gov.au)